

1 Atmospheric methane control mechanisms during the early 2 Holocene

3 Ji-Woong Yang¹, Jinho Ahn¹, Edward J. Brook², and Yeongjun Ryu¹

4 ¹School of Earth and Environmental Sciences, Seoul National University, Seoul 08826, South Korea

5 ²College of Earth, Ocean, and Atmospheric Sciences, Oregon State University, Corvallis, OR 97331, USA

6 *Correspondence to:* Jinho Ahn (jinhoahn@snu.ac.kr)

7 **Abstract.** Understanding processes controlling the atmospheric methane (CH₄) mixing ratio is crucial to predict
8 and mitigate future climate changes in this gas. Despite recent detailed studies of the last ~1000 to 2000 years,
9 the mechanisms that control atmospheric CH₄ still remain unclear, partly because the late Holocene CH₄ budget
10 may be comprised of both natural and anthropogenic emissions. In contrast, the early Holocene was a period when
11 human influence was substantially smaller, allowing us to elucidate more clearly the natural controls under
12 interglacial conditions more clearly. Here we present new high resolution CH₄ records from Siple Dome,
13 Antarctica, covering from 11.6 to 7.7 thousands of years before 1950 AD (ka). We observe four local CH₄ minima
14 on a roughly 1000-year spacing, which correspond to cool periods in Greenland. We hypothesize that the cooling
15 in Greenland forced the Intertropical Convergence Zone (ITCZ) to migrate southward, reducing rainfall in
16 northern tropical wetlands. The inter-polar difference (IPD) of CH₄ shows a gradual increase from the onset of
17 the Holocene to ~9.5 ka, which implies growth of boreal source strength following the climate warming in the
18 northern extratropics during that period.

19 1 Introduction

20 Methane (CH₄) is a potent greenhouse gas whose atmospheric mixing ratio has increased more than 2.5 times
21 since the Industrial Revolution (Dlugokencky et al., 2009). Although lower in abundance compared to carbon
22 dioxide (CO₂), CH₄ has ~28 times higher global warming potential (GWP) on a 100 year time scale and even
23 higher GWP on shorter time scales due to its short atmospheric lifetime (Stocker et al., 2013). Hence
24 understanding the controls on atmospheric CH₄ is important to predict and mitigate future climate and
25 environmental changes.

26 Naturally, CH₄ is mainly produced from microbial decomposition by methanogens in anaerobic environments,
27 such as waterlogged soil, wetlands, or sediments of lakes and rivers. Even though a part of CH₄ is oxidized, and
28 can be emitted in the form of CO₂, a considerable amount of CH₄ is still released into the atmosphere through
29 vascular plants, diffusion and ebullition processes (e.g., Joabsson and Christensen, 2001). Other, more minor
30 sources include geological CH₄ released from mud volcanoes and gas seepages through faults (e.g., Etiope et al.,
31 2008 and references therein), pyrogenic sources such as wildfire and biomass burning (Andreae and Merlet, 2001;
32 Ferretti et al., 2005; Hao and Ward, 1993), and microbial digestion by wild animals and termites (e.g., Sanderson,
33 1996). The CH₄ flux from the ocean to the atmosphere is considered as too small to create a significant change in
34 global budget compared to the other sources (e.g., Rhee et al., 2009). The major sink of atmospheric CH₄ is

1 photochemical reactions (oxidation) with the hydroxyl radical (OH), which is mainly controlled by atmospheric
2 temperature, humidity, and the mixing ratio of CH₄ itself and non-methane volatile organic compound (NMVOC)
3 (e.g., Levine et al., 2011 and references therein). Air temperature affects humidity thereby limiting the production
4 of OH. Oxidation of both NMVOCs and CH₄ compete for OH, that is, an increase in NMVOC emission reduces
5 the available OH, and increases the atmospheric lifetime of CH₄ (Valdes et al., 2005). Further, since the OH is
6 produced by photo-dissociation reaction, the CH₄ sink strength is affected by light availability and tropospheric
7 ozone (e.g., Levy, 1971). However, recent model studies suggested that CH₄ changes between glacial- and
8 interglacial conditions were driven mostly by source changes, rather than sink changes (Weber et al., 2010; Levine
9 et al., 2011).

10 Polar firn and ice are the unique archives that preserve the ancient atmosphere for the research of fossil air
11 older than the 20th century. Paleoatmospheric CH₄ levels have been reconstructed for the last 800 ka from
12 Antarctic- and Greenland ice cores (Loulergue et al., 2008). Given the relatively long lifetime in troposphere (11.2
13 ± 1.3 years at present, e.g., Prather et al., 2012) compared to atmospheric mixing time, ice core CH₄ records
14 represent well-mixed global signatures. The 800 ka record, shows that past CH₄ change generally followed
15 glacial-interglacial cycles, with low concentrations during glacial periods and high concentrations in interglacials,
16 as well as the shorter orbital cycles of obliquity and precession (e.g., Spahni et al., 2005; Loulergue et al., 2008).
17 Those earlier studies suggested that the changes in climate and hydrology in the tropics induced by orbital forcing
18 controlled CH₄ emissions. The resemblance between water stable isotope records from Greenland ice cores, a
19 proxy for Greenland temperature change, and global CH₄ mixing ratios on millennial time scales is also well
20 known. This implies that local temperature change around Greenland is linked to the major CH₄ sources in low
21 latitudes (e.g., Brook et al., 1996; Chappellaz et al., 1993; Huber et al., 2006; EPICA Community Members, 2006;
22 Grachev et al., 2007, 2009).

23 Intensive precipitation changes in the low latitude summer monsoon regions, caused by insolation changes (e.g.,
24 Asian monsoon) have been suggested as an important CH₄ control during the glacial period (e.g., Chappellaz et
25 al., 1990). From time series analysis of past CH₄ records, Guo et al. (2012) found that the tropical monsoon
26 circulation is a primary control of relatively shorter (millennial) time scale variability, while long-term (multi-
27 millennial to orbital scale) variations are dominated by solar insolation changes. It has been found that tropical
28 monsoon activity is closely related to orbital-scale CH₄ change (e.g., Brook et al., 1996; Chappellaz et al., 1990),
29 especially Asian monsoon (e.g., Loulergue et al., 2008) and South American monsoon (e.g., Cruz et al., 2005).
30 However, no direct correlation between CH₄ and tropical monsoon signals has been reported for the early
31 Holocene, although positive relationships between Greenland climate and tropical monsoon intensity (e.g., Chiang
32 et al., 2008), as well as between Greenland climate and CH₄ (e.g., Spahni et al., 2005; Wang et al., 2005; Mitchell
33 et al., 2011) have been reported.

34 The relationship between the latitudinal shift of the ITCZ and CH₄ emissions varies with time scales. Landais
35 et al. (2010) and Guo et al. (2012) suggested that ITCZ migration is not a dominant control of glacial-interglacial
36 CH₄ cycle because long-term CH₄ trend does not follow the precessional insolation change in the northern
37 hemisphere (NH) well. Modelling studies found the southward shift of the ITCZ coincides with reduced CH₄ in
38 Last Glacial Maximum (LGM) and Heinrich Stadial (HS) events, even though changes in wetland area and surface
39 hydrology were limited (Weber et al., 2010; Hopcroft et al., 2011). These authors instead suggested that changes
40 in temperature and/or plant productivity affected CH₄ production during those events. ITCZ migration does appear

1 to be related to millennial- or sub-millennial scale CH₄ change, however. Brook et al. (2000) found that sub-
2 millennial CH₄ minima during the last deglaciation correspond with reduced precipitation recorded in Cariaco
3 Basin sediment data, which indicates southward displacement of ITCZ (Hughen et al., 1996). This hypothesis is
4 supported by spectral analysis of CH₄ during the past 800 ka record that found that ITCZ change becomes an
5 important driver of millennial scale CH₄ change (Tzedakis et al., 2009; Guo et al., 2012).

6 For the Holocene, high-resolution CH₄ records from Law Dome and West Antarctic Ice Sheet (WAIS) Divide
7 ice cores in Antarctica show characteristic variability on multi-decadal to centennial time scale during the late
8 Holocene (MacFarling-Meure et al., 2006; Mitchell et al., 2011). The high-resolution records have been compared
9 with various temperature- and precipitation proxies, but previous work found no strong correlations that explain
10 the observed decadal- to centennial scale variabilities. This may be because the late Holocene CH₄ budget was
11 comprised of both natural and anthropogenic terms, making it difficult to distinguish between them. Mitchell et
12 al. (2011) pointed out that some of the abrupt CH₄ decreases could have had anthropogenic causes. Later, Mitchell
13 et al. (2013) made simultaneous measurement of Antarctic (WAIS Divide) and Greenland (Greenland Ice Sheet
14 Project 2; GISP2) ice cores to derive an IPD record, and extended their high-resolution records back to ~4 ka.
15 They used eight-box atmospheric methane model (EBAMM) and anthropogenic- and natural emission scenarios
16 to investigate CH₄ control factors. Their results showed that the late Holocene CH₄ evolution can be explained by
17 a combination of natural- and anthropogenic emissions. In principle, stable isotope ratios of CH₄ help us to
18 distinguish the types of sources – biogenic, pyrogenic, and geologic. Sowers (2010) reconstructed the CH₄ mixing
19 ratio and stable isotopic composition ($\delta^{13}\text{C-CH}_4$ and $\delta\text{D-CH}_4$) throughout the entire Holocene. He suggested
20 several possible control factors, such as boreal wetlands and thermokarst lakes, changing C₃/C₄ plant ratio of CH₄-
21 emitting ecosystems, and changing composition of methanogenic communities. Previous studies have shown
22 reduction of pyrogenic emission and increased agricultural emission during the last millennium (Ferretti et al.,
23 2005; Mischler et al., 2009). In later work using $\delta^{13}\text{C-CH}_4$ records from North Greenland Eemian Ice Drilling
24 (NEEM) ice core, Sapart et al. (2012) found that the centennial-scale variations during the last two millennia were
25 caused by changes in pyrogenic- and biogenic emissions. Ruddiman et al. (2011) and Sapart et al. (2012) estimated
26 CH₄ emission change due to anthropogenic land use changes, which shows a good agreement with the trends from
27 ice core measurement. Since there is no high-resolution reconstruction of past population and land use area, and
28 consequently large uncertainties of CH₄ emission from land use change impede identification of any shorter scale
29 changes.

30 The early Holocene is a suitable period to study natural CH₄ controls under Holocene interglacial climate
31 condition. Since there was only negligible human population and relevant CH₄-emitting anthropogenic activities
32 (e.g., Goldewijk et al., 2010; Kaplan et al., 2011) during this time, the early Holocene CH₄ changes must have
33 occurred mostly due to natural causes. Understanding natural controls could contribute to better constraints on
34 human-induced CH₄ changes. However, high-resolution studies that covers the entire early Holocene have not
35 been carried out extensively so far, except for studies of the prominent cooling event at 8200 years BP (Spahni et
36 al., 2003; Kobashi et al., 2007; Ahn et al., 2014). Despite Rhodes et al. (2015) reported a very high-resolution
37 record from WAIS Divide ice core that extends from the last glacial period to the earliest Holocene (~9.8 ka), the
38 authors do not deal with the early Holocene CH₄ variability. Earlier studies mainly focused on long-term change,
39 attributing the major control to low latitude hydrology based on regional climate records that show wetter climate
40 in tropics during the early Holocene (Blunier et al., 1995; Brook et al., 2000; Chappellaz et al., 1993, 1997).

1 Therefore, in this study we present a new high-resolution CH₄ record from the early Holocene and investigate
2 natural control mechanisms under interglacial condition. It should be noted that environmental boundary
3 conditions of the early Holocene were not identical to those of the late Holocene. Global sea level rose throughout
4 the early Holocene while remnant ice sheets in North America disappeared.

5 **2 Materials and Methods**

6 In this study we used ice samples from the Siple Dome deep ice core (SDMA) drilled from 1997 to 1999 on the
7 Siple Coast, West Antarctica (81.65°S, 148.81°W; 621 m elevation) (Taylor et al., 2004). The SDMA samples
8 were collected and cut at National Ice Core Laboratory (NICL, Denver, Colorado, USA) from January to February
9 of 2013. The brittle zone of SDMA ice starts below 400 m and continues to the bottom of the core at 1004 m
10 (Gow and Meese, 2007) and samples from this region are more likely to be fractured. Hence, the samples were
11 carefully collected from unbroken subsections during sample preparation at NICL. The samples were packed in
12 insulated foam boxes with numerous eutectic gels, and shipped to South Korea via expedited airfreight.
13 Temperature loggers showed the temperatures were maintained below -25°C. The boxes were picked up directly
14 just after custom clearance at the airport and then the ice samples were stored in a walk-in freezer at Seoul National
15 University (SNU, Seoul, South Korea) that was maintained below -20°C. We measured 295 individual ice samples
16 from 156 depth intervals from 518.87 to 718.83 m, covering from 8.36 to 20.25 ka after synchronizing to the
17 Greenland Ice Core Chronology 2005 (GICC05, Rasmussen et al., 2006), of which 256 ice samples from 120
18 depth intervals from 518.87 to 623.38 m are used in this study. All samples were duplicated, so that our final CH₄
19 data were presented by averaging the results of duplicate analysis from the same depth. The analytical uncertainty
20 of our data set is estimated by the uncertainty of individual ice measurement divided by square root of 2 (see
21 below). We rejected data that show difference between duplicate measurements larger than 10 ppb, and 9 data
22 points were rejected in the studied period. The results of SNU measurement (111 points) are plotted in Figure 1.
23 The 16 samples from 8 depths were used for reproducibility check on different days (Table 1). The air occluded
24 in ice was extracted by a melting and refreeze process under vacuum. Ice samples were prepared in a walk-in
25 freezer in the morning of each experiment day, the outermost >2 mm was trimmed off to eliminate potential
26 contamination by ambient air during the storage. The samples were then moved to the laboratory and placed in
27 glass sample containers. The sample flasks were custom-made glass flasks welded to stainless steel flanges, and
28 attached to the vacuum line with copper gaskets. The sample flasks were partially submerged in a chilled ethanol
29 bath while being attached to the vacuum line. Flasks were evacuated for at least 40 minutes, then the ice samples
30 were melted by submerging the sample flasks in a warm water bath. Melting was usually completed within 30
31 minutes. The sample flasks were then submerged in the cold ethanol bath chilled to around -82°C for more than
32 an hour to refreeze. During refreezing, we carried out daily calibration of the gas chromatograph system, normally
33 taking ~90 minutes. The ethanol temperature normally rose to -55°C just after submerging the flasks, and
34 recovered to -65°C before expansion of the air in the flasks. The extracted air in the headspace was expanded into
35 the evacuated vacuum line and sample loop of a gas chromatograph (GC) equipped with a flame ionization
36 detector (FID) to measure CH₄ mixing ratio. After detecting the CH₄ peak in the GC chromatogram (retention
37 time of ~1.6 minutes), the vacuum line and sample loop is evacuated again prior to the next injection. The GC
38 linearity was tested by a series of inter-tank calibration using four working standard air cylinders (395.5, 721.3,

1 895.0, and 1384.9 ppb CH₄ on NOAA04 scale, Dlugokencky et al., 2005). A daily GC calibration curve was
2 determined by measurements of a working standard having the closest CH₄ mixing ratio of expected value from
3 the samples; in this study, we used the 721.3 ppb CH₄ standard for samples of the early Holocene. We calibrated
4 with a standard air six times before and after sample measurements. The detailed configuration of the vacuum line
5 and GC is described in another paper (Yang et al., in preparation).

6 Different solubilities of each air component cause preferential dissolution during melting procedure. As the
7 solubility of CH₄ is higher than the other major components of air – nitrogen (N₂), oxygen (O₂), Argon (Ar), the
8 CH₄ mole fraction of the extracted air is lower than originally enclosed air (solubility effect). The CH₄ mole
9 fraction of air enclosed in ice sample is estimated from residual gas fraction and CH₄ mixing ratio in air remained
10 in refrozen meltwater (retrapped air). Residual gas fraction is a measure of how much air is retrapped during
11 refreeze, which is defined as ratio of amount (pressure) of air extracted from the 2nd gas extraction to the 1st
12 extraction. The 2nd gas extraction was carried out using leftover refrozen meltwater samples after the 1st extraction
13 finished. Mean residual gas fraction is $1.05 \pm 0.13\%$ (1σ , $n = 60$) for SDMA ice samples and $0.38 \pm 0.08\%$ (1σ , n
14 $= 40$) for bubble-free ice. The test with ice samples from Styx glacier, Antarctica revealed that CH₄ mixing ratio
15 in retrapped air is enriched 3.1 times ($n = 12$) for glacial ice and 3.0 times ($n = 7$) for bubble-free ice. Then the
16 solubility effect is corrected by using a simple mass balance calculation.

17 Daily systematic offset correction was applied to account for the daily-varying system condition. To do this,
18 we measured four bubble-free ice samples every day with SDMA ice samples. The experimental procedures for
19 the bubble-free ice were identical to the SDMA ice. After the sample flasks are evacuated, standard air is injected
20 into the flasks containing bubble-free ice, so that it returns similar air pressure to the typical size of SDMA ice
21 when the extracted air inside the bubble-free ice flasks is expanded into the sample loop. The solubility correction
22 for the bubble-free ice was done by the same formula as SDMA ice samples, but using different residual gas
23 fraction. After corrected for solubility effect, the daily systematic offset is calculated by difference between CH₄
24 mixing ratio of the injected standard air and results from the four flasks containing bubble-free ice. The systematic
25 offset ranges from 5 to 15 ppb during the SDMA measurement period. A daily offset is subtracted from the ice
26 samples corrected for gas solubility effect. This is one of the major differences with OSU wet extraction system,
27 where the systematic offset is interpolated from the results of blank tests carried out between several days
28 (Mitchell et al., 2011).

29 The bubble-free ice was made by chilling the degassed ultrapure water (resistivity $>18.2 \text{ M}\Omega\cdot\text{cm}$ at 25°C)
30 slowly from the bottom in a closed stainless steel chamber. From gas extraction test using our bubble-free ice
31 without injecting standard air, we observed that no significant pressure increase at the pressure gauge with a
32 detection limit of 0.01 Torr (corresponding to less than 0.03% of sample air pressure in the extraction line) after
33 melting-refreezing the bubble-free ice. Mass dependent (gravitational) fractionation within the firm (Craig et al.,
34 1988; Schwander, 1989) was corrected by using the nitrogen isotope ratio ($\delta^{15}\text{N}$) of atmospheric N₂ occluded in
35 bubbles. Siple Dome $\delta^{15}\text{N}$ records show a mean enrichment of $0.23 \pm 0.01\%$ during the early Holocene
36 (Severinghaus et al., 2009) and result in a slight decrease of CH₄ by 1.97 ± 0.15 ppb, which we applied to all of
37 our measurements.

38 Here we consider two types of uncertainty sources: uncertainty in (1) estimating daily systematic offset and (2)
39 other causes. The former indicates uncertainty of the daily systematic offset ($e1$). As the daily systematic offset is
40 calculated from the mean of the four flasks with bubble-free ice and standard air, scattering of the bubble-free ice

1 samples can induce uncertainty in the systematic offset correction. The daily $e1$ is estimated with standard error
2 of the mean (SEM, $n=4$), because the daily systematic offset is calculated from the mean of the four bubble-free
3 ice samples. The average of daily $e1$ is 1.9 ppb. The latter ($e2$) includes uncertainty due to solubility correction
4 and inhomogeneous distribution of CH_4 . Given our solubility correction uses the mean value of residual gas
5 fraction and the ratio at which CH_4 enriches in retrapped air, different solubility effect and/or inhomogeneous CH_4
6 distribution in individual ice causes offset between adjacent duplicate ice samples analysed on the same day. As
7 the duplicates from same depths were measured on the same day, we estimated the $e2$ with pooled standard
8 deviation (PSD) between duplicate measurements from entire depths, which yields 3.3 ppb. Taking the $e1$ and $e2$
9 into account together, the final uncertainty of individual measurement is given as 3.8 ppb by error propagation.
10 The uncertainty for the mean of duplicate results is obtained by dividing the individual uncertainty by square root
11 of 2, yielding 2.7 ppb. Further details on the correction method is found in our manuscript in preparation (Yang
12 et al., in preparation).

13 We made additional measurements using adjacent samples (depth difference of 10 cm) at randomly selected 8
14 depth intervals to examine reproducibility and long-term stability of our system. The second measurements of
15 duplicates were performed 8 to 80 days after the first analysis. Table 1 displays quadruplicate results at each depth.
16 PSD between the mean of duplicate analyses of the first and second measurements on different days yields 1.1
17 ppb. The good agreement between duplicate means indicates good reproducibility of our system. In the meanwhile,
18 PSD of the quadruplicate measurements is 3.0 ppb, which is similar to PSD of duplicate samples for the entire
19 data set (3.3 ppb).

20 To check reliability of the record we compared our data set with previous SDMA measurements at Oregon
21 State University (OSU) for 8.4 to 9.1 ka period when the two records overlap. The OSU CH_4 record was
22 measured with a temporal resolution of 8 years with precision of 2.8 ppb (Mitchell et al., 2011; Ahn et al., 2014).
23 The average offset between the two data sets is 0.1 ppb, which lies within analytical uncertainty range of data sets.
24 Therefore, we created a composite record by using the OSU data for 499.49 – 537.20 m interval (7.6 to 9.0 ka)
25 because mean temporal resolution of OSU data (~22 years) is lower than SNU data (~37 years) during this period
26 (Fig. 1). Our new SDMA CH_4 composite data have mean temporal resolution of ~26 years. The WAIS Divide
27 continuous CH_4 records show much higher resolution (~2 years), but does not cover the entire early Holocene
28 period (Rhodes et al., 2015).

29 **3. Result and Discussion**

30 **3.1 Millennial scale variability**

31 We carried out spectral analysis of SDMA composite record using the REDFIT program (Schulze and Mudelsee,
32 2002). Moderate (over 90% significance level) spectral power was found at ~1340, 401, 309, and 96-year periods.
33 Given the ~42 years of gas age distribution of SDMA (Ahn et al., 2014), it would not reliable to study centennial
34 scale variability. Therefore, we smoothed the data by a 250-year running average to remove centennial- to multi-
35 centennial scale components and then detrended by a high-pass filter with a cut off period of 1800 years to isolate
36 millennial scale variability. For comparison, the same processing scheme was applied to WAIS Divide time series

1 and we observed that Siple Dome and WAIS Divide CH₄ anomalies share similar millennial scale variability,
2 confirming the reliability of both our data and observed millennial scale changes (Fig. 2).

3 The high-pass filtered CH₄ time series demonstrates millennial scale minima at ~8.2, 9.3, 10.2 and 10.9 ka,
4 which occurred with nearly 1000-year spacing. The REDFIT results for 7.6 to 11.2 ka interval that excludes PBO
5 shows moderate (80% significance level) powers at ~731 and 430 (860)-year periods. Each minimum is
6 accompanied by depletion of water stable isotope ratio ($\delta^{18}\text{O}_{\text{ice}}$) from North Greenland Ice Core Project (NGRIP)
7 ice core, which implies climate cooling in Greenland. A close relationship between CH₄ and Greenland $\delta^{18}\text{O}_{\text{ice}}$
8 has been previously reported in glacial-interglacial cycles and Dansgaard-Oeschger (DO) events during the last
9 glacial period (e.g., Brook et al., 1996, 2000; Blunier and Brook, 2001; Chappellaz et al., 1993, 2013; EPICA
10 Community Members, 2006). However, it has not been confirmed for interglacial climate conditions during the
11 Holocene. Mitchell et al. (2011) found no significant correlation with Greenland climate in multi-decadal scale
12 during the late pre-industrial Holocene (LPIH), possibly because LPIH CH₄ budget is also affected substantially
13 by anthropogenic emissions (e.g., Ferretti et al., 2005; Mischler et al., 2009; Mitchell et al., 2013; Sapart et al.,
14 2012). In contrast, we observe a significant positive correlation ($r = 0.57$, $p = 0.06$) between the millennial-scale
15 change of Siple Dome CH₄ and NGRIP $\delta^{18}\text{O}_{\text{ice}}$ during the early Holocene. The correlation coefficient between the
16 smoothed- and filtered time series of SDMA CH₄ (before synchronization to GICC05) and NGRIP $\delta^{18}\text{O}_{\text{ice}}$ was
17 calculated for the 7.8 - 11.5 ka by interpolating to the original ages of SDMA CH₄ composite, with a reduced
18 degree of freedom.

19 The gas chronology of SDMA was developed based on CH₄ and $\delta^{18}\text{O}$ of air ($\delta^{18}\text{O}_{\text{atm}}$) correlation (Severinghaus
20 et al., 2009). In this study, we improved the chronology by synchronization of the previous chronology to GICC05
21 age scale by setting 3 age tie-points with stable water isotope ($\delta^{18}\text{O}$) record from the North Greenland Ice Core
22 Project (NGRIP) ice cores during the abrupt climate change events of the Preboreal Oscillation (PBO) and the 8.2
23 ka event, given that both events have been proved to be synchronous with CH₄ change (Kobashi et al., 2007,
24 2008). Ages between tie-points were inferred by linear interpolation of the age offset of nearest tie-points, which
25 range from -114 to 28 years. After synchronizing to the GICC05 scale, the correlation coefficient between SDMA
26 CH₄ composite and the NGRIP $\delta^{18}\text{O}_{\text{ice}}$ increases to $r = 0.74$ ($p < 0.01$) It implies that natural CH₄ budget is closely
27 connected with Greenland climate on millennial timescales, even though this conclusion is less robust as there is
28 no age tie-points between the 8.2 ka episode and PBO (Fig. 3). The positive correlation implies that the natural
29 CH₄ budget is connected with Greenland climate on millennial timescales.

30 The uncertainty of the modified chronology was examined by comparing with a tentative age scale determined
31 by CH₄ correlation with NEEM CH₄ discrete measurement data. NEEM CH₄ data follow GICC05modelext-
32 NEEM-1 scale (Rasmussen et al., 2013). The detailed method for CH₄ correlation is described in Section 3.2. The
33 age difference between the two chronologies is plotted in Figure 4, showing the maximum age difference of 105
34 years. In addition, we include the maximum layer counting uncertainty of 99 years (Rasmussen et al., 2006) and
35 delta-age uncertainty of 30 years (Rasmussen et al., 2013) during the early Holocene. Therefore, error propagation
36 of the above three errors indicate that the maximum error of SDMA gas age used in this study is ~147 years.

37 According to atmospheric modelling studies, abrupt cooling in the North Atlantic regions can alter atmospheric
38 circulation and to cause southward migration of the mean latitudinal position of the ITCZ (e.g., Chiang and Bitz,

1 2005; Broccoli et al., 2006; Cvijanovic and Chiang, 2012). Climate proxies demonstrate the climatic
2 teleconnection between northern North Atlantic and low latitude regions. Sediment reflectance record from
3 Cariaco Basin shows increased rainfall and humidity – which is due to southward displacement of ITCZ –
4 corresponding to the 8.2, 9.3, and 10.9 ka abrupt cooling event, as revealed in previous studies for the different
5 time periods (Peterson et al., 2000; Haug et al., 2001; Fleitmann et al., 2007; Deplazes et al., 2013). The southward
6 displacement of the ITCZ leads further weakening of Asian and Indian summer monsoons and probably reduces
7 CH₄ emission from northern tropical wetlands. The ¹⁸O enrichment in speleothems from Dongge Cave (China),
8 Qunf Cave (Oman), and Hoti Cave (Oman, not shown, Neff et al., 2001) occurred at similar timing with abrupt
9 cooling in Greenland at 8.2, 9.3, and 10.9 ka, which indicates the reduction of monsoonal rainfall in northern
10 tropical wetlands. The speleothem records from Chinese and Oman caves seem to lag by ~100 – 200 years after
11 the CH₄ change at ~9.3 ka, but this lies within chronological uncertainties of ~200 – 400 years at around ~9.0 ka
12 (Dykoski et al., 2005; Fleitmann et al., 2007). Moreover, sediment Ba/Ca ratio from Gulf of Guinea demonstrates
13 concurrent decrease of West African monsoon (Weldeab et al., 2007). In contrast, an inverse relationship is
14 observed from the Eastern Brazilian speleothem data (Lapa Grande Cave, Strikis et al., 2011) that suggest an
15 increase in precipitation at the time of abrupt CH₄ decreases. Rhodes et al. (2015) pointed out that strong
16 southward migration of the ITCZ could induce an abrupt CH₄ increase from southern hemisphere (SH) during the
17 HS 1, 2, 4, and 5 events. Sperlich et al. (2015) also suggested that a sharp CH₄ peak at Greenland Interstadial 21.2
18 (~85 ka) was caused by emission from Asian and Amazon wetlands. However, considering the orbital parameters
19 that indicate maximum summer insolation in NH while minimum in SH during the early Holocene, it can be
20 inferred that contribution of SH wetland emission was relatively weak and overcompensated by reduction of NH
21 emission.

22 The possibility that the observed CH₄ minima were caused by reduction of northern extra-tropical sources is
23 not supported by previous modelling studies. Zürcher et al. (2013) found that abrupt cooling in Greenland and
24 northern high latitudes by large freshwater input to the North Atlantic causes boreal peatland CH₄ emission to
25 decrease substantially, which can explain ~23% of abrupt CH₄ decrease (~80 ppb) during the 8.2 ka event. Given
26 the meltwater pulses during the early Holocene before the 8.2 ka event were probably much weaker (Teller and
27 Leverington, 2004) than that corresponding to the 8.2 ka event, we suggest that boreal emission change is not the
28 major cause of the CH₄ local minima.

29 Previously, Björck et al. (2001) found that climate cooling in the northern Atlantic and Santa Barbara Basin
30 occurred associated with a change in solar-forcing at ~10.3 ka. However, the proxy data in Figure 2 show no clear
31 indication of southward migration of the ITCZ and changes in Asian, Indian, African, and South American
32 summer monsoon intensity associated with the ~10.2 ka cooling and CH₄ decrease. (Fig. 2b-f). Furthermore,
33 speleothem $\delta^{18}\text{O}$ records from Mawmluh Cave (not shown) show no weakening of the Indian monsoon
34 (Berkelhammer et al., 2012), and there was no distinct change in $\Delta\epsilon_{\text{LAND}}$, a proxy of global terrestrial respiratory
35 fractionation of atmospheric O₂ at this time, which is affected by low latitude surface hydrology (Severinghaus et
36 al., 2009). These evidences suggest that precipitation and surface hydrology in the northern tropics may have not
37 changed significantly during around the 10.2 ka. Instead, there are two small decreases at ~9.9 and ~10.6 ka as
38 shown in Dongge cave deposit record (Fig. 2d), but it is difficult to tell, given dating uncertainties, if these events
39 correlate with the 10.2 ka cooling. Although there appears to have been no strong change in low latitude hydrology
40 at 10.2 ka, the amplitude of CH₄ decrease at 10.2 ka is similar order to the other millennial events. Given that no

1 clear reduction of the Asian, Indian, and African monsoon intensity is observed, it is possible that the CH₄
2 decrease at 10.2 ka was controlled by other processes, outside of the northern tropics.

3 Previous studies have suggested an important role of solar forcing during the Holocene (e.g., Björck et al., 2001;
4 Bond et al., 1997, 2001). Bond et al. (1997) reported four large ice-rafted debris (IRD) drifts occurred at ~8.1, 9.4,
5 10.3 and 11.1 ka caused by surface cooling of North Atlantic Ocean. They found that the ocean surface cooling
6 and the IRD events are closely related to cooling over the Greenland. Figure 2 shows that each IRD event (maxima
7 in hematite stained grain) occurred concurrently with minima of NGRIP $\delta^{18}\text{O}_{\text{ice}}$ record within age uncertainty. We
8 postulate that the Greenland cooling leads to southward shift of the ITCZ and in turn it changes wetland CH₄
9 emission in low latitudes. Bond et al. (2001) found that IRD maxima during the Holocene coincide with solar
10 activity minima and suggested that solar forcing could affect the climate change around the North Atlantic Ocean
11 (and Greenland), through amplification by changes in sea ice and/or deep water formation. A close interplay
12 between solar activity and monsoon intensity has been observed in previous studies using the Chinese and Oman
13 speleothem records during the Holocene (Neff et al., 2001; Wang et al., 2005; Gupta et al., 2005), even on multi-
14 decadal time scales (Agnihotri et al., 2002). However, the forcing mechanism of solar activity on the North
15 Atlantic and global climate is not well understood. Jiang et al. (2015) found positive correlations between North
16 Atlantic SST and solar forcing inferred from paleo-proxies (¹⁴C and ¹⁰Be) for the last 4000 years, although the
17 correlation disappears during the mid- and early Holocene. They hypothesized that climate sensitivity to solar
18 forcing is high for cooler climate. The above evidence suggests that the early Holocene CH₄ minima may be linked
19 to anomalies in solar activity, but future study is needed to make it more conclusive.

20 Meanwhile, a shift to an El Niño-like SST state was suggested as another mechanism that changes tropical
21 rainfall patterns (Marchitto et al., 2010). According to modern atmospheric observations, El Niño conditions lead
22 to drying conditions in low latitude wetlands in Africa, Asia, and the Americas (e.g., Dai and Wigley, 2000; Lyon
23 and Barnston, 2005; Hodson et al., 2011), which reduces tropical CH₄ emissions. Thus, we could speculate that
24 both the ITCZ migration and El Niño-like SST change affected the tropical surface hydrology and CH₄ emission.
25 According to Holocene ENSO activity reconstructions by Moy et al. (2002), no ENSO event was recorded during
26 the early Holocene until around 7 ka, except weak ENSO events during 10.4 – 10.1 ka, where we observe a CH₄
27 drop apparently unrelated to monsoon proxies. Mitchell et al. (2011) observed a significant positive correlation
28 between CH₄ and Pacific Decadal Oscillation (PDO) variability during the late Holocene. It has been reported that
29 PDO modulates the wet/dry impact of ENSO depending on phase relationship between ENSO and PDO (e.g.,
30 Wang et al., 2014 and references therein). Using a Holocene PDO reconstruction from sediment grain size analysis
31 by Kirby et al. (2010) shows PDO-related drying intervals in North America during 9.5 – 9.1, 8.9 – 8.6, and 8.3
32 – 7.8 ka, which overlap the CH₄ minima at 8.2 and 9.3 ka present in this study.

33 **3.2 Inter-polar difference of CH₄ during the early Holocene**

34 We calculated the inter-polar difference (IPD) of CH₄ to trace the latitudinal source distribution change during
35 the early Holocene. The currently available high-resolution CH₄ records covering the early Holocene are SDMA
36 discrete (this study), WAIS Divide discrete (WAIS Divide project members, 2015), WAIS Divide continuous
37 (Rhodes et al., 2015), NEEM discrete (Chappellaz et al., 2013) and NEEM continuous data (Chappellaz et al.,
38 2013). Among the Antarctic records, we consider WAIS continuous records most reliable from ~9.9 to 11.5 ka

1 interval. For the rest of the studied period, SDMA discrete records are better constrained than WAIS discrete data,
2 because SDMA records have better analytical precision, as well as comparison with OSU measurements reveals
3 a minimal offset for the early Holocene interval. Before IPD calculation, WAIS continuous data were calibrated
4 to SDMA data, given the discrete measurements generally have better accuracy than continuous ones. Regarding
5 the Greenland side, we use NEEM discrete records because not only there are discrepancies between continuous-
6 and discrete data in some intervals, but also because NEEM discrete records were measured by similar wet
7 extraction technique at OSU (Chappellaz et al., 2013).

8 Precise synchronization is crucial for direct comparison between data sets which have high frequency variations.
9 For synchronizing between Antarctic (Siple Dome and WAIS Divide continuous) and NEEM records, the NEEM
10 CH₄ record (~11 years resolution on average) is chosen as reference. Synchronization was done by two steps:
11 First, we made initial synchronization between the Antarctic and NEEM data by setting match points at the
12 midpoint of abrupt CH₄ change, and then we linearly interpolated the age offset of each match point for the rest
13 of data points. Then we applied a Monte Carlo simulation to find a maximum correlation. Both data sets were
14 resampled every 30 years, and each point was randomly perturbed (assuming a normal distribution with 1 sigma
15 of 30 years). By doing so 1000 different time series were created, and the set having a maximum correlation with
16 NEEM data was chosen. Criteria for “best fit” is correlation coefficient of 0.8 with NEEM original age scale, so
17 that a maximum correlation less than 0.8 was discarded. This procedure was repeated to make 20 sets of maximum
18 correlation time series, and the mean ages of 20 replicate simulations were set to synchronized age scale. The
19 uncertainty range of IPD was calculated from synchronization uncertainty and CH₄ data uncertainty. To estimate
20 synchronization uncertainty, we created 20 IPDs from the 20 sets of maximum correlation time series, and the
21 standard deviation of the 20 records was taken as synchronization uncertainty for each of the data points. The CH₄
22 data uncertainty was estimated with the stated uncertainty of each data set (4.3 ppb for NEEM discrete / 2.7 ppb
23 for SDMA / 1.5 ppb for WAIS continuous, 1 sigma). To check the sensitivity of the uncertainties, we carried out
24 Monte Carlo simulations. We produced 1000 different sets of IPD, which vary randomly with Gaussian
25 propagation in their ages and CH₄ concentration uncertainties. Each IPD was annually interpolated and smoothed
26 by a 1/1000 year⁻¹ low-pass filter. The cutoff frequency of 1000 years was chosen to examine multi-centennial to
27 millennial scale change, because the IPD calculation is very sensitive to high frequency variability of CH₄ records
28 from both poles. To report 95% confidence interval, we multiplied the standard deviation by 1.96 and enveloped
29 the IPD.

30 Figure 6 displays the IPDs calculated from various pairs of data set with 95% significant interval. The two IPD
31 records derived from most reliable data sets are plotted in red (NEEM discrete – Siple Dome, IPD-1 hereafter)
32 and green (NEEM discrete – WAIS continuous, IPD-2 hereafter). Both IPD-1 and IPD-2 show a long-term
33 increase from 11.5 to 9.9 ka, which indicates that boreal source contribution enhanced. However, IPD-1 shows a
34 sharper increase during the PBO followed by decrease until ~10.7 ka, and in the latter case both IPDs differ beyond
35 95% envelope (from 10.4 to 10.8 ka). Although these differences are significant, and are probably due to small
36 errors in the time scale and absolute concentrations differences, for example, due to uncertainties in blank
37 corrections or solubility corrections, or core quality, they do not affect our basic interpretation of the trends.
38 Instead, we combined the two IPDs to resolve this. Given the IPD-2 is better constrained than IPD-1, we use IPD-
39 2 curve from 9.9 to 11.5 ka interval and IPD-1 for the rest of the studied period (Fig. 6). The combined IPD shows
40 ~13 ppb increase from 11.5 to 9.5 ka. It displays similar trend with the NH extratropical (30° - 90°N) temperature

1 reconstruction (Marcott et al., 2013) and the modelled CH₄ emission from boreal thermokarst lakes (Walter et al.,
2 2014), indicating that NH extratropical source strength increased during this period.

3 To quantify the source strength of low- and high latitude sources, we employed a simple 3-box CH₄ source
4 distribution model used in previous studies (Chappellaz et al., 1997; Brook et al., 2000). Briefly, the model
5 contains 3 boxes; northern extra-tropical latitude (30°N – 90°N, N-box), tropical (30°S – 30°N, T-box), and
6 southern extra-tropical latitude boxes (30°S – 90°S, S-box). CH₄ mixing ratios in 3 boxes (in Tg box⁻¹) were
7 determined from CH₄ mixing ratio of Antarctica and Greenland. The mean CH₄ mole fraction of N-box (30°N –
8 90°N) is not identical to that of Greenland ice core record, given the latitudinal CH₄ distribution (e.g., Fung et al.,
9 1991). To derive the N-box CH₄, we followed the assumption of Chappellaz et al. (1997), where the authors
10 assumed that difference between Greenland and the mean N-box CH₄ is 7% of IPD. Hence here the N-box CH₄
11 is calculated by subtracting 7% of IPD from the Greenland mixing ratio. T-box mixing ratio is inferred by
12 assuming that the S-box emission is constant of 15 Tg yr⁻¹ (Fung et al., 1991). Emission from each box (Tg yr⁻¹)
13 is then estimated by using the mixing ratios of the boxes, lifetime of CH₄ in each box, and transport times among
14 the boxes. Following Chappellaz et al. (1997), we assume the lifetime of 18.7, 8.1, and 26.8 years in N, T, and S-
15 box, respectively, and transport time of 9 months. The modelled emission changes are plotted in Figure 8. The
16 model results reveal that tropical sources decrease (accounting for the largest portion in CH₄ budget), while NH
17 extratropical emissions increase. The T-box emission is reduced from ~118 Tg yr⁻¹ to ~109 Tg yr⁻¹, and the N-
18 box source strength increases from ~60 Tg yr⁻¹ to ~71 Tg yr⁻¹ during the 11.5 – 9.5 ka interval (Fig. 8). The long-
19 term decrease of tropical emission follows the NH summer insolation change. This covariation may reflect the
20 insolation-driven changes in emissions on multi-millennial timescale (e.g., Loulergue et al., 2008; Guo et al.,
21 2012). Also plotted in Figure 8 is the boreal source fraction, defined as ratio of N-box emission to total source
22 emissions, showing 5% increase (from 31.5 to 36.5%) during the same interval. The box model results at 9.0, 9.5,
23 and 11.5 ka time slices are summarised in Table 2.

24 Our results are supported by proxy-based temperature reconstructions that indicate a gradual warming in
25 northern extratropical regions (30°N – 90°N) until ~9.6 ka, while tropical temperature remains stable (Marcott et
26 al., 2013). The climate warming in northern high latitudes caused ice sheet retreat (e.g., Dyke, 2004) and may
27 have enhanced CH₄ emission by forming new wetlands in permafrost regions (e.g., Gorham et al., 2007; Yu et al.,
28 2013) and accelerating microbial decomposition of organic material (e.g., Christensen et al., 2004; Schuur et al.,
29 2015). Thermokarst lakes created by thawing ice wedges and ground ice in Alaskan- and Siberian permafrost has
30 been suggested as a source of CH₄ (e.g., Walter et al., 2006, 2007; Brosius et al., 2012). The modelled
31 enhancement of NH extratropical emission of ~11 Tg yr⁻¹ is similar to the CH₄ release of 8.2 Tg yr⁻¹ from
32 thermokarst lake thawing, which is estimated based on present-day observations (Walter et al., 2014). Since most
33 thermokarst lakes are located in NH high latitude regions (e.g., Walter et al., 2006, 2014), it may support the box
34 model results. Our results are consistent with previous findings based on CH₄ stable isotope analysis. Fischer et
35 al. (2008) found that increase of boreal source contribution is required to explain the more depleted δ¹³C-CH₄
36 during Preboreal period than the Younger Dryas interval. Sowers (2010) extended the CH₄ isotopic ratio into the
37 entire Holocene and showed a gradual decrease of δ¹³C-CH₄ by ~2‰ from 10.5 to 4 ka, which was attributed to
38 progressive expansion of NH high latitude sources.

39

4. Conclusion and summary

We reconstructed a new high resolution CH₄ record during the early Holocene from Siple Dome ice core, Antarctica, to study millennial CH₄ variability and its natural controls under Holocene interglacial condition. The new Siple Dome record agrees well with previous records measured at OSU within analytical uncertainty, showing a mean difference of 0.1 ppb. By combining the two data sets, we present a SDMA CH₄ composite record covering from ~7.7 to 11.6 ka. We observed four millennial scale CH₄ minima having 10–20 ppb of amplitude with 300–400 years duration. It is found that these CH₄ minima were accompanied with Greenland cooling, changes in ITCZ position and reduced Asian and Indian monsoon intensities. The observed evidences suggest that low latitude hydro climate changes were closely related to millennial scale CH₄ minima. Further, this study presented the millennial scale change of IPD, which was calculated from high resolution discrete data set of NEEM and SDMA, and a continuous record of WAIS Divide. Here we reported that the IPD increased by ~13 ppb from the onset of the Holocene to ~9.5 ka following the temperature rise in NH extra-tropical regions. The three-box model demonstrates that NH extratropical emissions elevated by ~11 Tg yr⁻¹, while tropical emission was reduced by ~9 Tg yr⁻¹, resulting the increased contribution of the NH extra-tropical sources by ~5%.

Acknowledgements. Financial support was provided by the Basic Science Research Program through the National Research Foundation of Korea (NRF) (NRF-2015R1A2A2A01003888) and Korea Polar Research Institution (KOPRI) research grant (PD12010 and PE15010). This work was also supported by the US National Science Foundation Grant PLR 1043518. We appreciate all the efforts of sample cutting and shipping of the Siple Dome ice core by Brian Bencivengo, Richard Nunn, and Geoffrey Hargreaves of National Ice Core Laboratory, Denver, Colorado. We sincerely thank to Yoo-Hyeon Jin, Jinhwa Shin, and Hun-Gyu Lee for their laboratory assistance and helpful discussions. Thanks should go to Heejo Lee for her help in preparing English manuscript. We are grateful to Mark Twickler and the NICL Science Management Office for providing the Siple Dome ice core samples, the collection of which was supported by the US National Science Foundation.

Data availability

The early Holocene Siple Dome CH₄ data will be available on NOAA Paleoclimatology database and PANGAEA data repository.

References

- Agnihotri, R., Dutta, K., Bhushan, R., and Somayajulu, B. L. K.: Evidence for solar forcing on the Indian monsoon during the last millennium, *Earth Planet. Sci. Lett.*, 198, 521-527, 2002.
- Ahn, J., Brook, E. J., and Buizert, C.: Response of atmospheric CO₂ to the abrupt cooling event 8200 years ago, *Geophys. Res. Lett.*, 41, 604-609, 2014.
- Andreae, M. O., and Merlet, P.: Emission of trace gases and aerosols from biomass burning, *Global Biogeochem. Cycles*, 15, 955-966, 2001.
- Baumgartner, M., Kindler, P., Eicher, O., Floch, G., Schilt, A., Schwander, J., Spahni, R., Capron, E., Chappellaz, J., Leuenberger, M., Fischer, H., and Stocker, T. F.: NGRIP CH₄ concentration from 120 to 10 kyr before

1 present and its relation to a $\delta^{15}\text{N}$ temperature reconstruction from the same ice core, *Clim. Past*, 10, 903-920,
2 2014.

3 Berger, A., and Loutre, M. F.: Insolation values for the climate of the last 10 million years, *Quat. Sci. Rev.*, 10,
4 297-317, 1991.

5 Berkelhammer, M., Sinha, A., Stott, L., Cheng, H., Pausata, F., and Yoshimura, K.: An abrupt shift in the Indian
6 Monsoon 4000 years ago, *Geophys. Monogr. Ser.*, 198, 75-87, 2012.

7 Björck, S., Muscheler, R., Kromer, B., Andresen, C. S., Heinemeier, J., Johnsen, S. J., Conley, D., Koç, N., Spurk,
8 M., and Veski, S.: High-resolution analyses of an early Holocene climate event may imply decreased solar
9 forcing as an important climate trigger, *Geology*, 29, 1107-1110, 2001.

10 Blunier, T., Chappellaz, J., Schwander, J., Stauffer, B., and Raynaud, D.: Variations in atmospheric methane
11 concentration during the Holocene epoch, *Nature*, 374, 46-49, 1995.

12 Blunier, T., and Brook, E. J.: Timing of millennial-scale climate change in Antarctica and Greenland during the
13 last glacial period, *Science*, 291, 109-112, 2001.

14 Broccoli, A. J., Dahl, K. A., and Stouffer, R. J.: Response of the ITCZ to northern hemisphere cooling, *Geophys.*
15 *Res. Lett.*, 33, L01702, 2006.

16 Bond, G., Kromer, B., Beer, J., Muscheler, R., Evans, M. N., Showers, W., Hoffmann, S., Lotti-Bond, R., Hajdas,
17 I., and Bonani, G.: Persistent solar influence on north Atlantic climate during the Holocene, *Science*, 294, 2130-
18 2136, 2001.

19 Brook, E. J., Sowers, T., and Orchardo, J.: Rapid variations in atmospheric methane concentration during the past
20 110,000 years, *Science*, 273, 1087-1091, 1996.

21 Brook, E. J., Harder, S., Severinghaus, J. P., Steig, E. J., and Sucher, C. M.: On the origin and timing of rapid
22 changes in atmospheric methane during the last glacial period, *Global Biogeochem. Cy.*, 14, 559-572, 2000.

23 Brook, E. J., White, J. W. C., Schilla, A. S. M., Bender, M. L., Barnett, B., Severinghaus, J. P., Taylor, K. C.,
24 Alley, R. B., and Steig, E. J.: Timing of millennial-scale climate change at Siple Dome, West Antarctica, during
25 the last glacial period, *Quat. Sci. Rev.*, 24, 1333-1343, 2005.

26 Brosius, L. S., Walter Anthony, K. M., Grosse, G., Chanton, J. P., Farquharson, L. M., Overduin, P. P., and Meyer,
27 H.: Using the deuterium isotope composition of permafrost meltwater to constrain thermokarst lake
28 contributions to atmospheric CH_4 during the last deglaciation, *J. Geophys. Res.*, 117, G01022, 2012.

29 Chappellaz, J., Blunier, T., Raynaud, D., Barnola, J. M., Schwander, J., and Stauffer, B.: Synchronous changes in
30 atmospheric CH_4 and Greenland climate between 40 and 8 kyr BP, *Nature*, 366, 443-445, 1993.

31 Chappellaz, J., Blunier, T., Kints, S., Dällenbach, A., Barnola, J. M., Schwander, J., Raynaud, D., and Stauffer,
32 B.: Changes in the atmospheric CH_4 gradient between Greenland and Antarctica during the Holocene, *J.*
33 *Geophys. Res.*, 102, 15987-15997, 1997.

34 Chappellaz, J., Stowasser, C., Blunier, T., Baslev-Clausen, D., Brook, E. J., Dallmayr, R., Faïn, X., Lee, J. E.,
35 Mitchell, L. E., Pascual, O., Romanini, D., Rosen, J., and Schüpbach, S.: High-resolution glacial and deglacial
36 record of atmospheric methane by continuous-flow and laser spectrometer analysis along the NEEM ice core,
37 *Clim. Past*, 9, 2579-2593, 2013.

38 Chiang, J. C. H., and Bitz, C. M.: Influence of high latitude ice core on the marine intertropical convergence zone,
39 *Clim. Dynam.*, 25, 477-496, 2005.

- 1 Chiang, J. C. H., Cheng, W., and Bitz, C. M.: Fast teleconnections to the tropical Atlantic sector from Atlantic
2 thermohaline adjustment, *Geophys. Res. Lett.*, 35, L07704, 2008.
- 3 Christensen, T. R., Johansson, T., Jonas Åkerman, H., Mastepanov, M., Malmer, N., Friberg, T., Crill, P., and
4 Svensson, B. H.: Thawing sub-arctic permafrost: effects on vegetation and methane emissions, *Geophys. Res.*
5 *Lett.*, 31, L04501.
- 6 Cvijanovic, I., and Chiang, J. C. H.: Global energy budget changes to high latitude North Atlantic cooling and the
7 tropical ITCZ response, *Clim. Dynam.*, 40, 1435-1452, 2013.
- 8 Craig, H., Horibe, Y., and Sowers, T.: Gravitational separation of gases and isotopes in polar ice caps, *Science*,
9 242, 1675-1678, 1988.
- 10 Cruz, F. W., Burns, S. J., Karmann, I., Sharp, W. D., Vuille, M., Cardoso, A. O., Ferrari, J. A., Silva Dias, P. L.,
11 and Viana, O.: Insolation-driven changes in atmospheric circulation over the past 116,000 years in subtropical
12 Brazil, *Nature*, 63-66, 2005.
- 13 Dai, A., and Wigley, T. M. L.: Global patterns of ENSO-induced precipitation, *Geophys. Res. Lett.*, 27, 1283-
14 1286, 2000.
- 15 Deplazes, G., Luckge, A., Peterson, L. C., Timmermann, A., Hamann, Y., Hughen, K. A., Rohl, U., Laj, C., Cane,
16 M. A., Sigman, D. M., and Haug, G. H.: Links between tropical rainfall and North Atlantic climate during the
17 last glacial period, *Nat. Geosci.*, 6, 213-217, 2013.
- 18 Dlugokencky, E. J., Steele, L. P., Lang, P. M., and Masarie, K. A.: The growth rate and distribution of atmospheric
19 methane, *J. Geophys. Res.*, 99, 17021-17043, 1994.
- 20 Dlugokencky, E. J., Myers, R. C., Lang, P. M., Masarie, K. A., Crotwell, A. M., Thoning, K. W., Hall, B. D.,
21 Elkins, J. W., and Steele, L. P.: Conversion of NOAA atmospheric dry air CH₄ mole fractions to a
22 gravimetrically prepared standard scale. *J. Geophys. Res.*, 110, 2005.
- 23 Dlugokencky, E. J., Bruhwiler, L., White, J. W. C., Emmons, L. K., Novelli, P. C., Montzka, S. A., Masarie, K.
24 A., Lang, P. M., Crotwell, A. M., Miller, J. B., and Gatti, L. V.: Observational constraints on recent increases
25 in the atmospheric CH₄ burden, *Geophys. Res. Lett.*, 36, L18803, 2009.
- 26 Dlugokencky, E.J., Nisbet, E. J., Fisher, R., and Lowry, D.: Global atmospheric methane: Budget, changes, and
27 dangers, *Philosophical Transactions of the Royal Society A*, 369, 2058-2072, 2011.
- 28 Dyke, A. S.: An outline of North American deglaciation with emphasis on central and northern Canada, in:
29 Quaternary Glaciations - Extent and Chronology Part II: North America, Volume 2, edited by: Ehlers J. and
30 Gibbard, P. L., Elsevier, Amsterdam, 373-424, 2004.
- 31 Dykoski, C. A., Edwards, R. L., Cheng, H., Yuan, D., Cai, Y., Zhang, M., Lin, Y., Qing, J., An, Z., and Revenaugh,
32 J.: A high-resolution, absolute-dated Holocene and deglacial Asian monsoon record from Dongge Cave, China,
33 *Earth Planet. Sci. Rev.*, 233, 71-86, 2005.
- 34 EPICA Community Members: One-to-one coupling of glacial climate variability in Greenland and Antarctica,
35 *Nature*, 444, 195-198, 2006.
- 36 Etiope, G., Lassey, K. R., Klusman, R. W., and Boschi, E.: Reappraisal of the fossil methane budget and related
37 emission from geologic sources, *Geophys. Res. Lett.*, 35, L09307, 2008.
- 38 Ferretti, D., Miller, J. B., White, J. W. C., Etheridge, D. M., Lassey, K. R., Lowe, D. C., MacFarling-Meure, C.
39 M., Dreier, M. F., Trudinger, C. M., van Ommen, T. D., and Langenfelds, R. L.: Unexpected changes to the
40 global methane budget over the past 2000 years, *Science*, 309, 1714-1717, 2005.

1 Finkel, R. C., and Nishizumi, K.: Beryllium 10 concentrations in the Greenland Ice Sheet Project 2 ice core from
2 3-40 ka, *J. Geophys. Res.*, 102, 26699-26706, 1997.

3 Fischer, H., Behrens, M., Bock, M., Richter, U., Schmitt, J., Loulergue, L., Chappellaz, J., Spahni, R., Blunier, T.,
4 Leuenberger, M., and Stocker, T. F.: Changing boreal methane sources and constant biomass burning during
5 the last termination, *Nature*, 452, 864-867, 2008.

6 Fleitmann, D., Burns, S. J., Mangini, A., Mudelsee, M., Kramers, J., Villa, I., Neff, U., Al-Subbary, A. A.,
7 Buettner, A., Hippler, D., and Matter, A.: Holocene ITCZ and Indian monsoon dynamics recorded in
8 stalagmites from Oman and Yemen (Socotra), *Quaternary Sci. Rev.*, 26, 170-188, 2007.

9 Flückiger, J., Blunier, T., Stauffer, B., Chappellaz, J., Spahni, R., Kawamura, K., Schwander, J., Stocker, T. F.,
10 and Dahl-Jensen, D.: N₂O and CH₄ variations during the last glacial epoch: Insight into global processes, *Global*
11 *Biogeochem. Cycles*, 18, GB1020, 2004.

12 Fung, I., John, J., Lerner, J., Matthews, E., Prather, M., Steele, L. P., and Fraser, P. J.: Three-dimensional model
13 synthesis of the global methane cycle, *J. Geophys. Res.*, 96, 13033-13065, 1991.

14 Goldewijk, K. K., Beusen, A., and Janssen, P.: Long-term dynamic modelling of global population and built-up
15 area in a spatially explicit way: HYDE 3.1, *The Holocene*, 1-9, 2010.

16 Gorham, E., Lehman, C., Dyke, A., Janssens, J., and Dyke, L.: Temporal and spatial aspects of peatland initiation
17 following deglaciation in North America, *Quaternary Sci. Rev.*, 26, 300-311, 2007.

18 Gow, A. J., and Meese, D.: Physical properties, crystalline textures and *c*-axis fabrics of the Siple Dome
19 (Antarctica) ice core, *J. Glaciol.*, 53, 573-584, 2007.

20 Grachev, A. M., Brook, E. J., and Severinghaus, J. P.: Abrupt changes in atmospheric methane at the MIS 5b-5a
21 transition, *Geophys. Res. Lett.*, 34, L20703, 2007.

22 Grachev, A. M., Brook, E. J., Severinghaus, J. P., and Piasias, N. G.: Relative timing and variability of atmospheric
23 methane and GISP2 oxygen isotopes between 68 and 86 ka, *Global Biogeochem. Cy.*, 23, GB2009, 2009.

24 Guillevic, M., Bazin, L., Landais, A., Stowasser, C., Masson-Delmotte, V., Blunier, T., Eynaud, F., Falourd, S.,
25 Michel, E., Minster, B., Popp, T., Prié, F., and Vinther, B. M.: Evidence for a three-phase sequence during
26 Heinrich Stadial 4 using a multi-proxy approach based on Greenland ice core records, *Clim. Past*, 10, 2115-
27 2133, 2014.

28 Guo, Z., Zhou, X., and Wu, H.: Glacial-interglacial water cycle, global monsoon and atmospheric methane
29 changes, *Clim. Dynam.*, 39, 1073-1092, 2012.

30 Gupta, A. K., Das, M., and Anderson, D. M.: Solar forcing on the Indian summer monsoon during the Holocene,
31 *Geophys. Res. Lett.*, 32, L17703, 2005.

32 Hao, W. M., and Ward, D. E.: Methane production from global biomass burning, *J. Geophys. Res.*, 98, 20657-
33 20661, 1993.

34 Haug, G. H., Hughen, K. A., Sigman, D. M., Peterson, L. C., and Röhl, U.: Southward migration of the
35 intertropical convergence zone through the Holocene, *Science*, 293, 1304-1308, 2001.

36 Hodson, E. L., Poulter, B., Zimmermann, N. E., Prigent, C., and Kaplan, J. O.: The El Niño-Southern Oscillation
37 and wetland methane interannual variability, *Geophys. Res. Lett.*, 38, L08810, 2011.

38 Hopcroft, P. O., Valdes, P. J., and Beerling, D. J.: Simulating idealized Dansgaard-Oeschger events and their
39 potential impacts on the global methane cycle, *Quat. Sci. Rev.*, 30, 3258-3268, 2011.

1 Hughen, K. A., Overpeck, J. T., Peterson, L. C., and Trumbore, S.: Rapid climate changes in the tropical Atlantic
2 region during the last deglaciation, *Nature*, 380, 51-54, 1996.

3 Jiang, H., Muscheler, R., Björck, S., Seidenkrantz, M. S., Olsen, J., Sha, L., Sjolte, J., Eriksson, J., Ran, L.,
4 Knudsen, K. L., and Knudsen, M. F.: Solar forcing of Holocene summer sea-surface temperatures in the
5 northern North Atlantic, *Geology*, 43, 2015.

6 Joabsson, A., and Christensen, T. R.: Methane emissions from wetlands and their relationship with vascular plants:
7 an Arctic example, *Global Change Biol.*, 7, 919-932, 2001.

8 Kaplan, J. O., Krumhardt, K. M., Ellis, E. C., Ruddiman, W. F., Lemmen, C., and Goldewijk, K. K.: Holocene
9 carbon emissions as a result of anthropogenic land cover change, *The Holocene*, 21, 775-791, 2011.

10 Kirby, M. E., Lund, S. P., Patterson, W. P., Anderson, M. A., Bird, B. W., Ivanovici, L., Monarrez, P., and Nielsen,
11 S.: A Holocene record of Pacific Decadal Oscillation (PDO)-related hydrologic variability in Southern
12 California (Lake Elsinore, CA), *J. Paleolimnol.*, 44, 819-839, 2010.

13 Kobashi, T., Severinghaus, J. P., Brook, E. J., Barnola, J. -M., and Grachev, A. M.: Precise timing and
14 characterization of abrupt climate change 8200 years ago from air trapped in polar ice, *Quaternary Sci. Rev.*,
15 26, 1212-1222, 2007.

16 Kobashi, T., Severinghaus, J. P., and Barnola, J. -M.: 4 ± 1.5 °C abrupt warming 11270 yr ago identified from
17 trapped air in Greenland ice, *Earth Planet. Sci. Lett.*, 268, 397-407, 2008.

18 Landais, A., Dreyfus, G., Capron, E., Masson-Delmotte, V., Sanchez-Goñi, M. F., Desprat, S., Hoffmann, G.,
19 Jouzel, J., Leuenberger, M., and Johnsen, S.: What drives the millennial and orbital variations of $\delta^{18}\text{O}_{\text{atm}}$?, *Quat.*
20 *Sci. Rev.*, 29, 235-246, 2010.

21 Levine, J. G., Wolff, E. W., Jones, A. E., Sime, L. C., Valdes, P. J., Archibald, A. T., Carver, G. D., Warwick, N.
22 J., and Pyle, J. A.: Reconciling the changes in atmospheric methane sources and sinks between the Last Glacial
23 Maximum and the pre-industrial era, *Geophys. Res. Lett.*, 38, L23804, 2011.

24 Levy II, H.: Normal atmosphere: large radical and formaldehyde concentrations predicted, *Science*, 173, 141-143,
25 1971.

26 Louergue, L., Schilt, A., Sphani, R., Masson-Delmotte, V., Blunier, T., Lemieux, B., Barnola, J. -M., Raynaud,
27 D., Stocker, T. F., and Chappellaz, J.: Orbital and millennial-scale features of atmospheric CH₄ over the past
28 800,000 years, *Nature*, 453, 383-386, 2008.

29 Lyon, B., and Barnston, A. G.: ENSO and the spatial extent of interannual precipitation extremes in tropical land
30 areas, *J. Clim.*, 18, 5095-5109, 2005.

31 MacDonald, G. M., Beilman, D. W., Kremenetski, K. V., Sheng, Y., Smith, L. C., and Velichko, A. A.: Rapid
32 early development of circumarctic peatlands and atmospheric CH₄ and CO₂ variations, *Science*, 314, 285-288,
33 2006.

34 MacFarling-Meure, C., Etheridge, D., Trudinger, C., Steele, P., Langenfelds, R., van Ommen, T., Smith, A., and
35 Elkins, J.: Law Dome CO₂, CH₄ and N₂O ice core records extended to 2000 years BP, *Geophys. Res. Lett.*, 33,
36 L14810, 2006.

37 Marchitto, T. M., Muscheler, R., Ortiz, J. D., Carriquiry, J. D., and van Geen, A.: Dynamical response of the
38 tropical Pacific Ocean to solar forcing during the early Holocene, *Science*, 330, 1378-1381, 2010.

39 Marcott, S. A., Shakun, J. D., Clark, P. U., and Mix, A. C.: A reconstruction of regional and global temperature
40 for the past 11300 years, *Science*, 339, 1198-1201, 2013.

1 Mischler, J. A., Sowers, T. A., Alley, R. B., Battle, M., McConnell, J. R., Mitchell, L., Popp, T., Sofen, E., and
2 Spencer, M. K.: Carbon and hydrogen isotopic composition of methane over the last 1000 years, *Global*
3 *Biogeochem. Cycles*, 23, GB4024, 2009.

4 Mitchell, L. E., Brook, E. J., Sowers, T., McConnell, J. R., and Taylor, K.: Multidecadal variability of atmospheric
5 methane, 1000–1800 C.E., *J. Geophys. Res.*, 116, G02007, 2011.

6 Mitchell, L. E., Brook, E. J., Lee, J. E., Buizert, C., and Sowers, T.: Constraints on the Late Holocene
7 anthropogenic contribution to the atmospheric methane budget, *Science*, 342, 964-966, 2013.

8 Moy, C.M., Seltzer, G. O., Rodbell, D. T., and Anderson, D. M.: Variability of El Niño/Southern Oscillation
9 activity at millennial timescales during the Holocene epoch, *Nature*, 420, 162-165, 2002.

10 Neff, U., Burns, S. J., Mangini, A., Mudelsee, M., Fleitmann, D., and Matter, A.: Strong coherence between solar
11 variability and the monsoon in Oman between 9 and 6 kyr ago, *Nature*, 411, 290-293 2001.

12 Petrenko, V. V., Smith, A. M., Brook, E. J., Lowe, D., Riedel, K., Brailsford, G., Hua, Q., Schaefer, H., Reeh, N.,
13 Weiss, R. F., Etheridge, D., and Severinghaus, J. P.: 14CH₄ measurements in Greenland ice: investigating last
14 glacial termination CH₄ sources, *Science*, 324, 506-508, 2009.

15 Prather, M. J., Holmes, C. D., and Hsu, J.: Reactive greenhouse gas scenarios: Systematic exploration of
16 uncertainties and the role of atmospheric chemistry, *Geophys. Res. Lett.*, 39, L0980, 2012.

17 Rasmussen, S. O., Andersen, K. K., Svensson, A. M., Steffensen, J. P., Vinther, B. M., Clausen, H. B., Siggaard-
18 Andersen, M. -L., Johnsen, S. J., Larsen, L. B., Dahl-Jensen, D., Bigler, M., Rothlisberger, R., Fischer, H.,
19 Goto-Azuma, K., Hansson, M. E., and Ruth, U.: A new Greenland ice core chronology for the last glacial
20 termination, *J. Geophys. Res.*, 111, D06102, 2006.

21 Rasmussen, S. O., Abbott, P. M., Blunier, T., Bourne, A. J., Brook, E., Buchardt, S. L., Buizert, C., Chappellaz,
22 J., Clausen, H. B., Cook, E., Dahl-Jensen, D., Davies, S. M., Guillevic, M., Kipstuhl, S., Laepple, T., Seierstad,
23 I. K., Severinghaus, J. P., Steffensen, J. P., Stowasser, C., Svensson, A., Vallenga, P., Vinther, B. M.,
24 Wilhelms, F., and Winstrup, M.: A first chronology for the North Greenland Eemian Ice Drilling (NEEM) ice
25 core, *Clim. Past*, 9, 2713-2730, 2013.

26 Renssen, H., Goosse, H., and Muscheler, R.: Coupled climate model simulation of Holocene cooling events:
27 oceanic feedback amplifies solar forcing, *Clim. Past*, 2, 79-90, 2006.

28 Rhee, T. S., Kettle, A. J., and Andreae, M. O.: Methane and nitrous oxide emissions from the ocean: A
29 reassessment using basin-wide observations in the Atlantic, *J. Geophys. Res.*, 114, D12304, 2009.

30 Rhodes, R. H., Brook, E. J., Chiang, J. C. H., Blunier, T., Maselli, O. J., McConnell, J. R., Romanini, D., and
31 Severinghaus, J. P.: Enhanced tropical methane production in response to iceberg discharge in the North
32 Atlantic, *Science*, 348, 1016-1019, 2015.

33 Ruddiman, W. F., Kutzbach, J. E., and Vavrus, S. J.: Can natural or anthropogenic explanations of late-Holocene
34 CO₂ and CH₄ increases be falsified?, *The Holocene*, 21, 865-879, 2011. Sanderson, M. G.: Biomass of termites
35 and their emissions of methane and carbon dioxide: A global database, *Global Biogeochem. Cy.*, 10, 543-558,
36 1996.

37 Sapart, C. J., Monteil, G., Prokopiou, M., van de Wal, R. S. W., Kaplan, J. O., Sperlich, P., Krumhardt, K. M.,
38 van der Veen, C., Houweling, S., Krol, M. C., Blunier, T., Sowers, T., Martinerie, P., Witrant, E., Dahl-Jensen,
39 D., and Röckmann, T.: Natural and anthropogenic variations in methane sources during the past two millennia,
40 *Nature*, 490, 85-88, 2012.

1 Schuur, E. A. G., McGuire, A. D., Schadel, C., Grosse, G., Harden, J. W., Hayes, D. J., Hugelius, G., Koven, C.
2 D., Kuhry, P., Lawrence, D. M., Natali, S. M., Olefeldt, D., Romanovsky, V. E., Schaefer, K., Turetsky, M. R.,
3 Treat, C. C., and Vonk, J. E.: Climate change and the permafrost carbon feedback, *Nature*, 520, 171-179.

4 Severinghaus, J. P., Beaudette, R., Headly, M. A., Taylor, K., and Brook, E. J.: Oxygen-18 of O₂ records the
5 impact of abrupt climate change on the terrestrial biosphere, *Science*, 324, 1431-1434, 2009.

6 Singarayer, J. S., Valdes, P. J., Friedlingstein, P., Nelson, S., and Beerling, D. J.: Late Holocene methane rise
7 caused by orbitally controlled increase in tropical sources, *Nature*, 470, 82-86, 2011.

8 Sowers, T.: Atmospheric methane isotope records covering the Holocene period, *Quat. Sci. Rev.*, 29, 213-
9 221, 2010.

10 Spahni, R., Schwander, J., Flückiger, J., Stauffer, B., Chappellaz, J. and Raynaud, D.: The attenuation of fast
11 atmospheric CH₄ variations recorded in polar ice cores, *Geophys. Res. Lett.*, 30, 1571, 2003.

12 Spahni, R., Chappellaz, J., Stocker, T. F., Loulergue, L., Hausammann, G., Kawamura, K., Flückiger, J.,
13 Schwander, J., Raynaud, D., Masson-Delmotte, V., and Jouzel, J.: Atmospheric methane and nitrous oxide of
14 late Pleistocene from Antarctic ice cores, *Science*, 310, 1317-1321, 2005.

15 Sperlich, P., Schaefer, H., Mikaloff Fletcher, S. E., Guillevic, M., Lassey, K., Sapart, C. J., Röckmann, T., and
16 Blunier, T.: Carbon isotope ratios suggest no additional methane from boreal wetlands during the rapid
17 Greenland Interstadial 21.2, *Global Biogeochem. Cycles*, 29, 1962-1976, 2015.

18 Stocker, T. F., Qin, D., Plattner, G.-K., Tignor, M., Allen, S. K., Boschung, J., Nauels, A., Xia, Y., Bex, V., and
19 Midgley, P. M. (Eds.): IPCC, 2013: Climate Change 2013: The Physical Science Basis, Contribution of
20 Working Group I to the Fifth Assessment Report of the Intergovernmental Panel on Climate Change,
21 Cambridge University Press, Cambridge, United Kingdom and New York, NY, USA, 1535 pp., 2013.

22 Taylor, K. C., Alley, R. B., Meese, D. A., Spencer, M. K., Brook, E. J., Dunbar, N. W., Finkel, R. C., Gow, A. J.,
23 Kurbatov, A. V., Lamorey, G. W., Mayewski, P. A., Meyerson, E. A., Nishiizumi, K., and Zielinski, G. A.:
24 Dating the Siple Dome (Antarctica) ice core by manual and computer interpretation of annual layering, *J.*
25 *Glaciol.*, 50, 453-461, 2004.

26 Tzedakis, P. C., Pälike, H., Roucoux, K. H., and de Abreu, L.: Atmospheric methane, southern European
27 vegetation and low-mid latitude links on orbital and millennial timescales, *Earth Planet. Sci. Lett.*, 277, 307-
28 317, 2009.

29 Valdes, P. J., Beerling, D. J., and Johnson, C. E.: The ice age methane budget, *Geophys. Res. Lett.*, 32, L02704,
30 2005.

31 Wang, Y., Cheng, H., Edwards, R. L., He, Y., Kong, X., An, Z., Wu, J., Kelly, M. J., Dykoski, C. A., and Li, X.:
32 The Holocene Asian monsoon: links to solar changes and north Atlantic climate, *Science*, 308, 854-857, 2005.

33 WAIS Divide Project Members: Precise inter-polar phasing of abrupt climate change during the last ice age, *Nature*,
34 520, 661-665, 2015.

35 Walter, K. M., Zimov, S. A., Chanton, J. P., Verbyla, D., and Chapin III, F. S.: Methane bubbling from Siberian
36 thaw lakes as a positive feedback to climate warming, *Nature*, 443, 71-75, 2006.

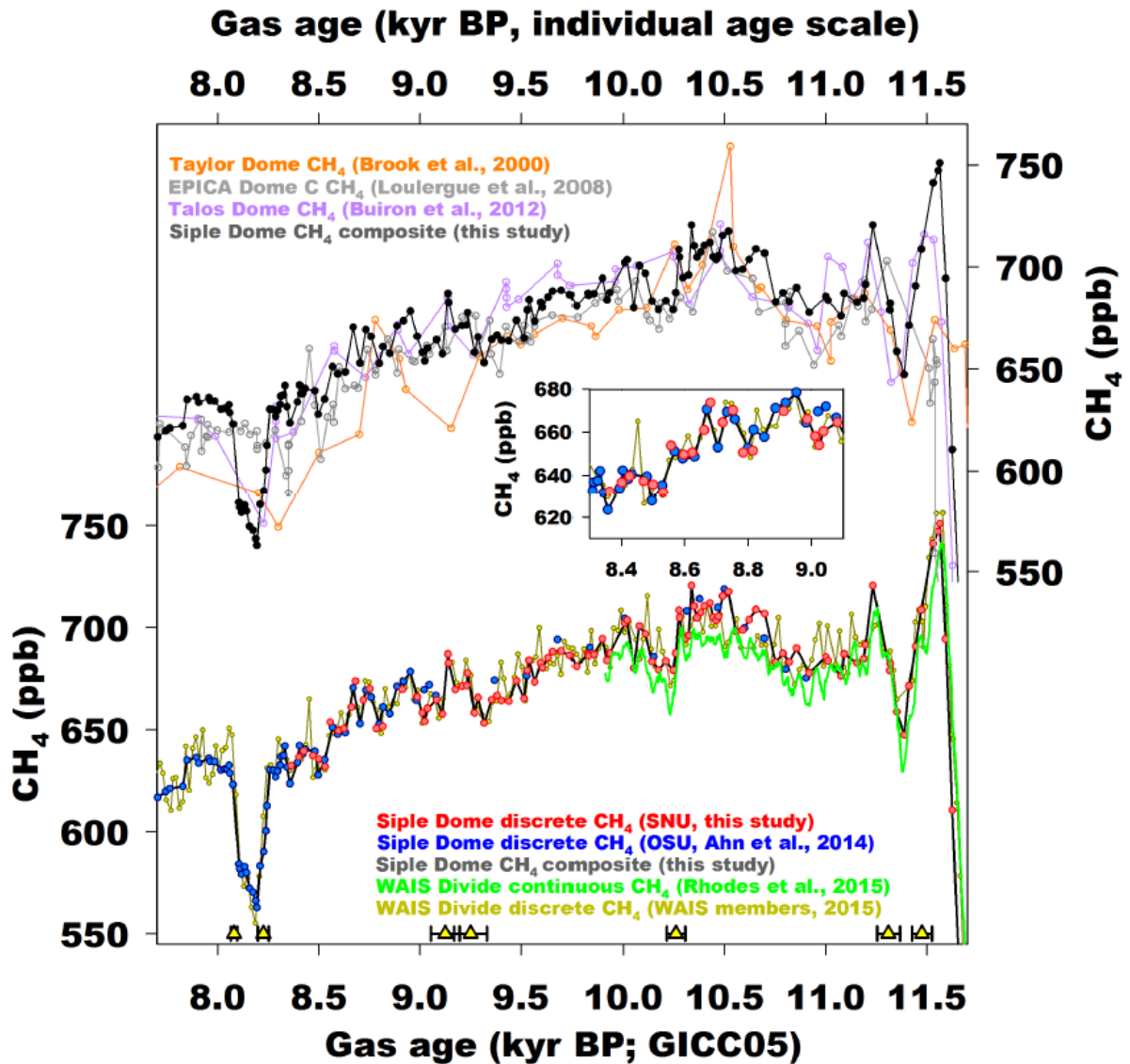
37 Walter, K. M., Edwards, M. E., Grosse, G., Zimov, S. A., and Chapin III, F. S.: Thermokarst lakes as a source of
38 atmospheric CH₄ during the last deglaciation, *Science*, 318, 633-636, 2007.

1 Walter Anthony, K. M., Zimov, S. A., Grosse, G., Jones, M. C., Anthony, P. M., Chapin III, F. S., Finlay, J. C.,
2 Mack, M. C., Davydov, S., Frenzel, P., and Frohking, S.: A shift of thermokarst lakes from carbon sources to
3 sinks during the Holocene epoch, *Nature*, 511, 452-456, 2014.

4 Weber, S. L., Drury, A. J., Toonen, W. H. J., and van Weele, M.: Wetland methane emissions during the Last
5 Glacial Maximum estimated from PMIP2 simulations: Climate, vegetation, and geographic controls, *J.*
6 *Geophys. Res.*, 115, D06111, 2010.

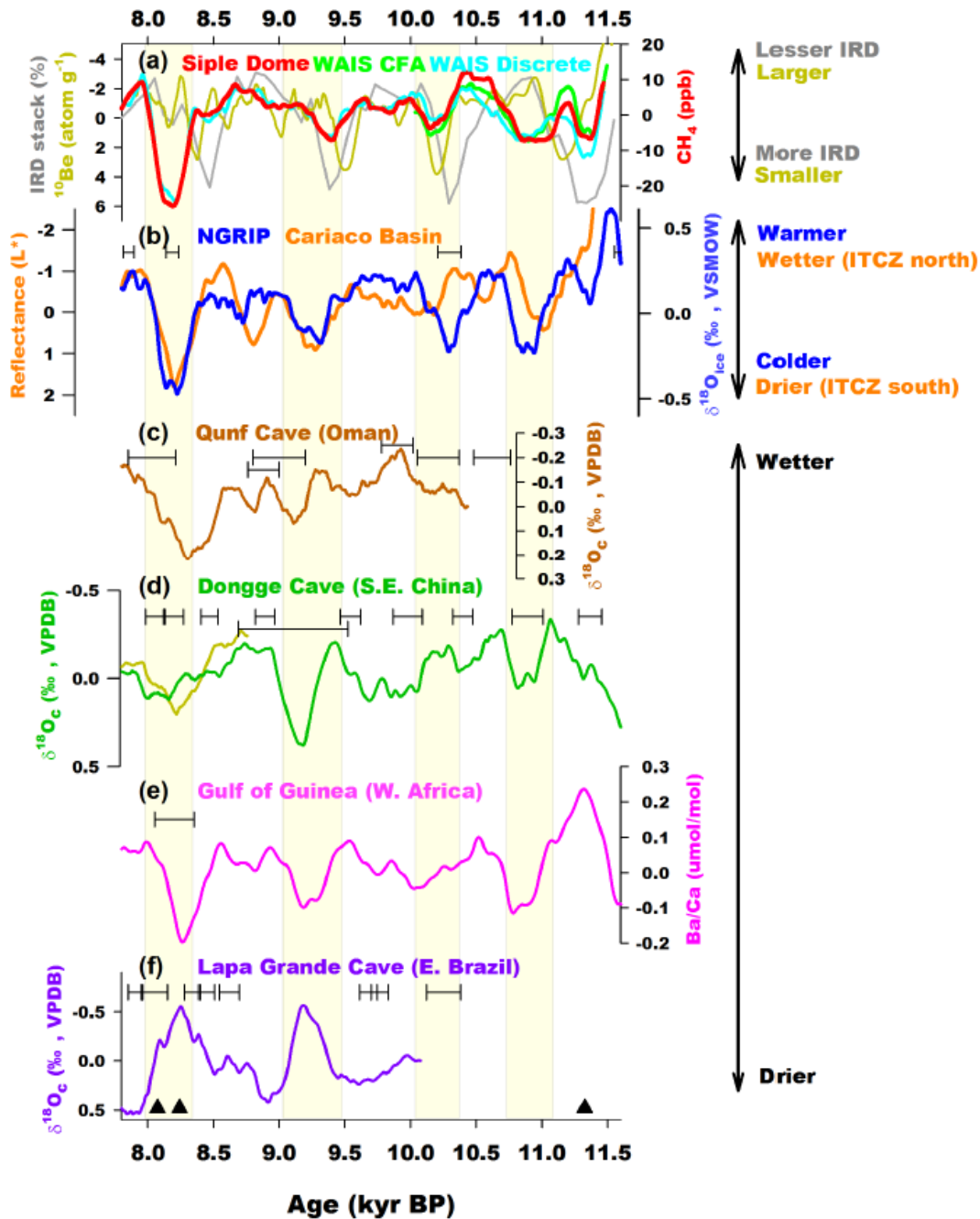
7 Yu, Z., Loisel, J., Turetsky, M. R., Cai, S., Zhao, Y., Frohking, S., MacDonald, G. M., and Bubier, J. L.: Evidence
8 for elevated emissions from high-latitude wetlands contributing to high atmospheric CH₄ concentration in the
9 early Holocene, *Global Biogeochem. Cy.*, 27, 1-10, 2013.

10



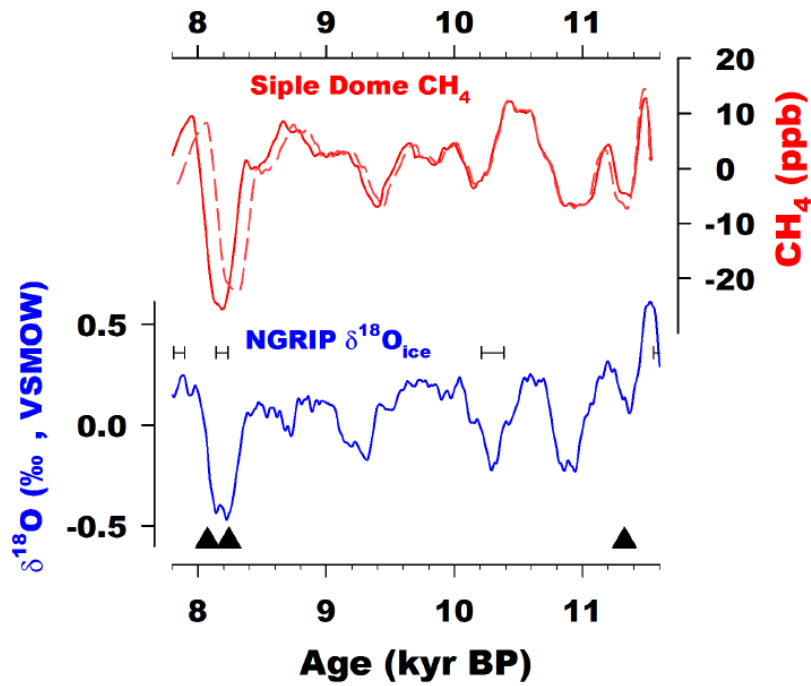
1
2 Figure 1. Atmospheric CH₄ concentration reconstructions during the early Holocene. Top: new high-resolution Siple
3 Dome composite (black, this study and Ahn et al., 2014) compared with previous records from Taylor Dome (orange,
4 Brook et al., 2000), EPICA Dome C (grey, Loulergue et al., 2008), and Talos Dome (purple, Buiron et al., 2012). Bottom:
5 Siple Dome CH₄ records measured at OSU (blue, Ahn et al., 2014) and SNU (red, this study). Siple Dome composite
6 (black line) is plotted with WAIS Divide discrete (dark yellow, WAIS Divide project members, 2015) and continuous
7 measurement records (green, Rhodes et al., 2015). Inset: Enlarged plot showing overlapped interval between OSU and
8 SNU Siple Dome data.

9



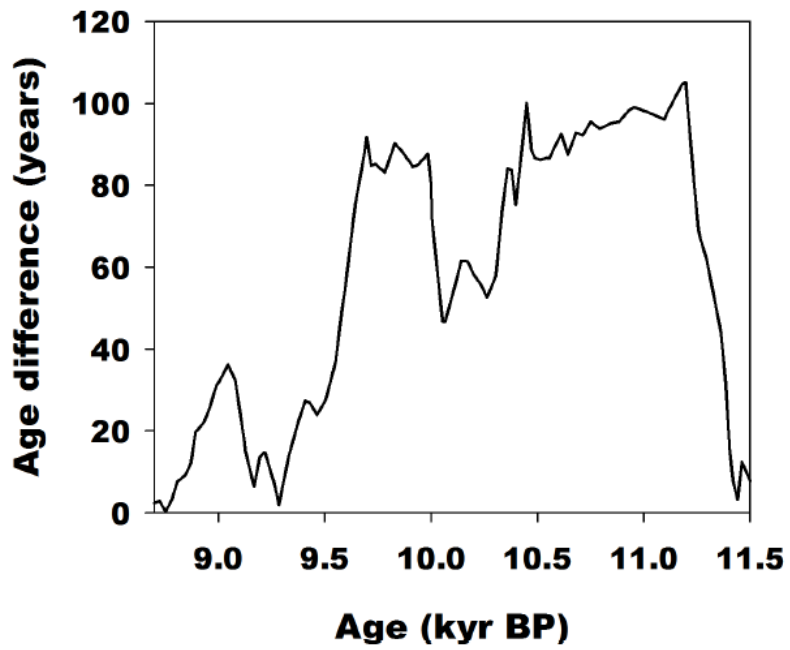
1
2
3
4
5
6
7
8
9
10
11

Figure 2. Millennial scale climate variability. All proxies presented here were smoothed by 250-year running average and detrended by high-pass filter with 1/1800-year window. (a) Siple Dome CH₄ (red, this study), Greenland ¹⁰Be (dark yellow, Finkel and Nishizumii, 1997), North Atlantic IRD stack (grey, Bond et al., 2001). Also shown are WAIS Divide CH₄ data by discrete (cyan, denoted “WAIS Discrete”, WAIS Divide project members, 2015) and continuous (yellow green, denoted “WAIS CFA”, Rhodes et al., 2015) technique. (b) NGRIP stable water isotope ratio (blue, Rasmussen et al., 2006) and Cariaco Basin reflectance (orange, Deplazes et al., 2013). (c) Qunf Cave speleothem oxygen isotope (Fleitmann et al., 2007). (d) Dongge Cave speleothem oxygen isotope (green, Dykoski et al., 2005; dark yellow, Wang et al., 2005). (e) Gulf of Guinea planktonic Ba/Ca ratio (Weldeab et al., 2007). (f) Lapa Grande Cave speleothem oxygen isotope (purple, Strikis et al., 2011). Black solid triangles are age tie-points used to adjust Siple Dome and WAIS Divide CH₄ data to GICC05 scale.



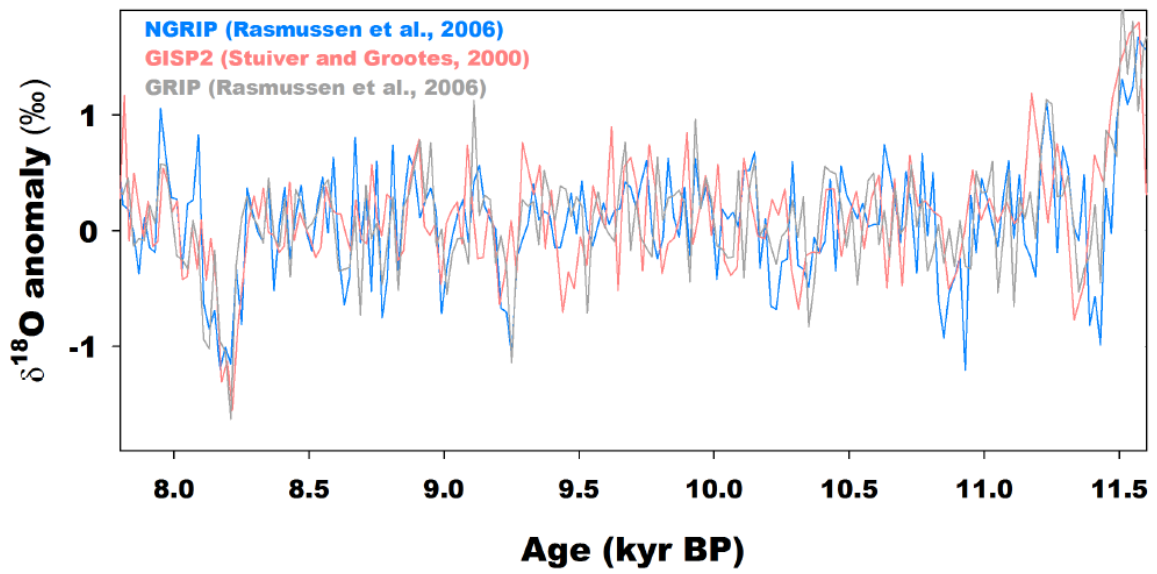
1
2
3
4
5
6
7

Figure 3. Upper: Comparison between Siple Dome CH₄ anomalies plotted with gas age adjusted to GICC05 (red, solid) and previous gas age (red, dashed; Brook et al., 2005). Lower: NGRIP δ¹⁸O anomaly in GICC05 scale. The horizontal error bars denote the age uncertainty of GICC05 chronology (Rasmussen et al., 2006), and the black triangles are age tie points used to adjusting the Siple Dome age scale to GICC05 scale.



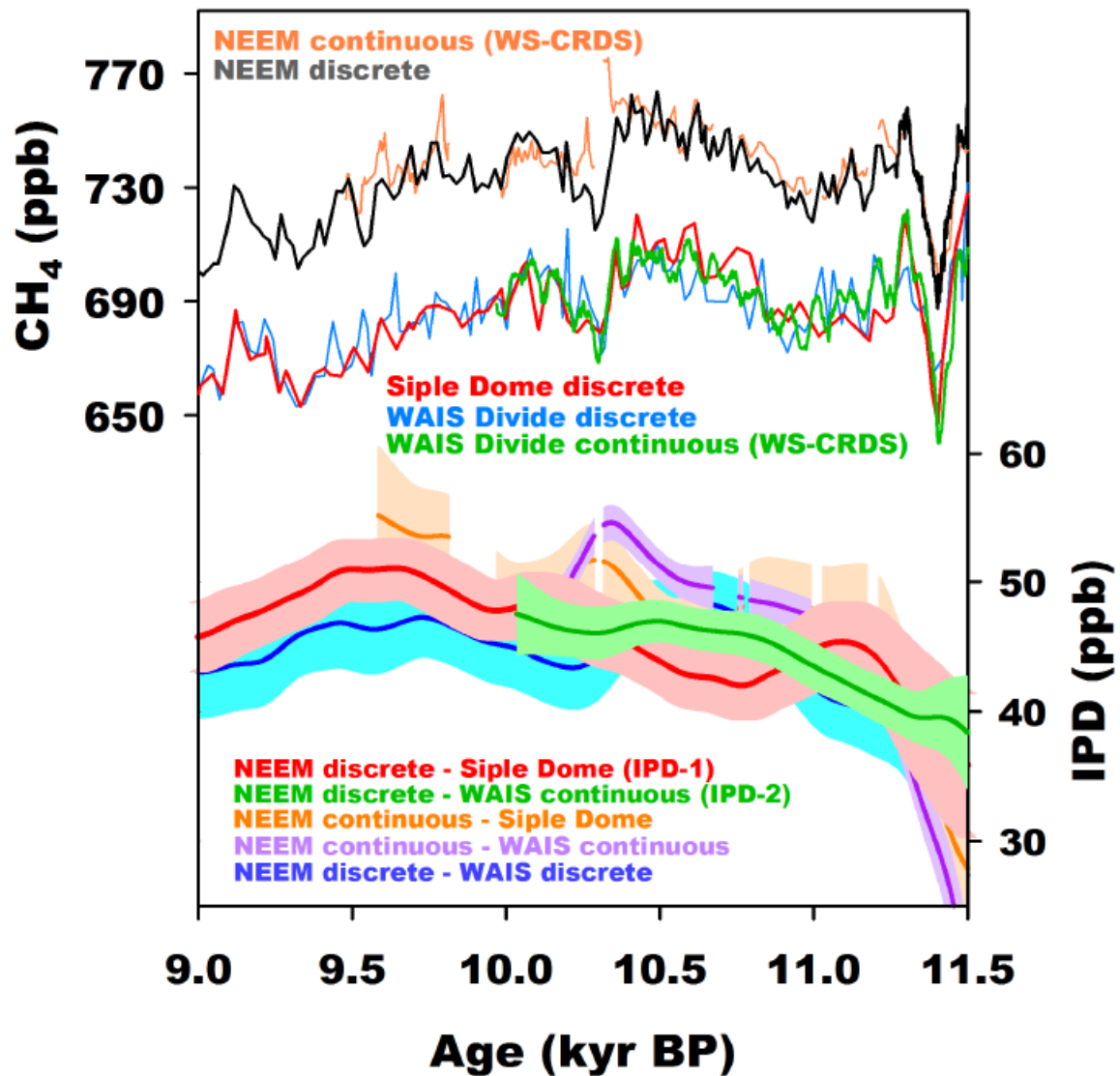
1

2 **Figure 4.** Age difference between the new gas age scale adjusted to GICC05 by Monte Carlo matching with NEEM
3 discrete CH₄ (Chappellaz et al., 2013) and the original gas age based on CH₄ and $\delta^{18}\text{O}_{\text{atm}}$ correlation (Severinghaus et
4 al., 2009).

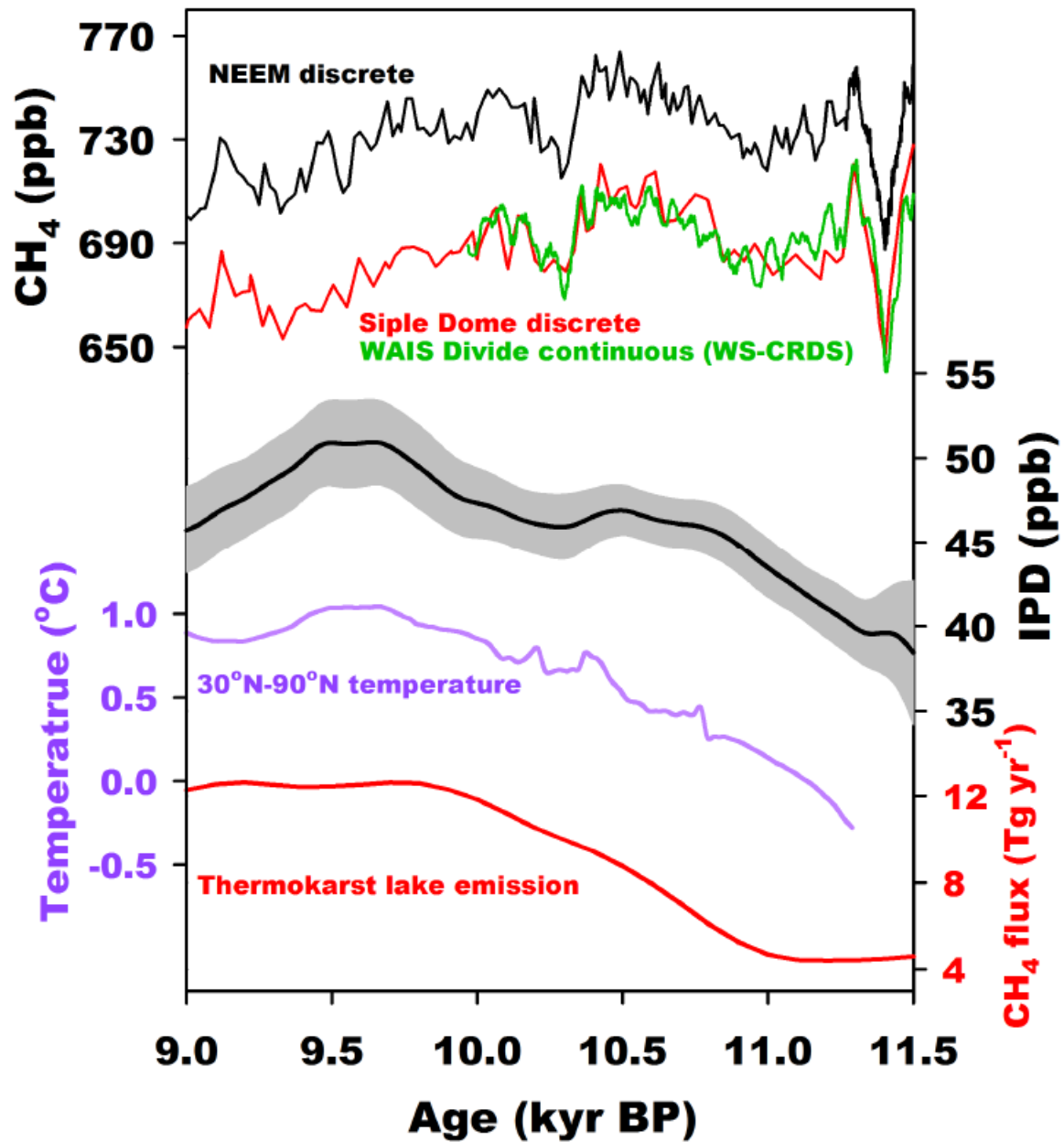


1
2
3
4
5
6
7

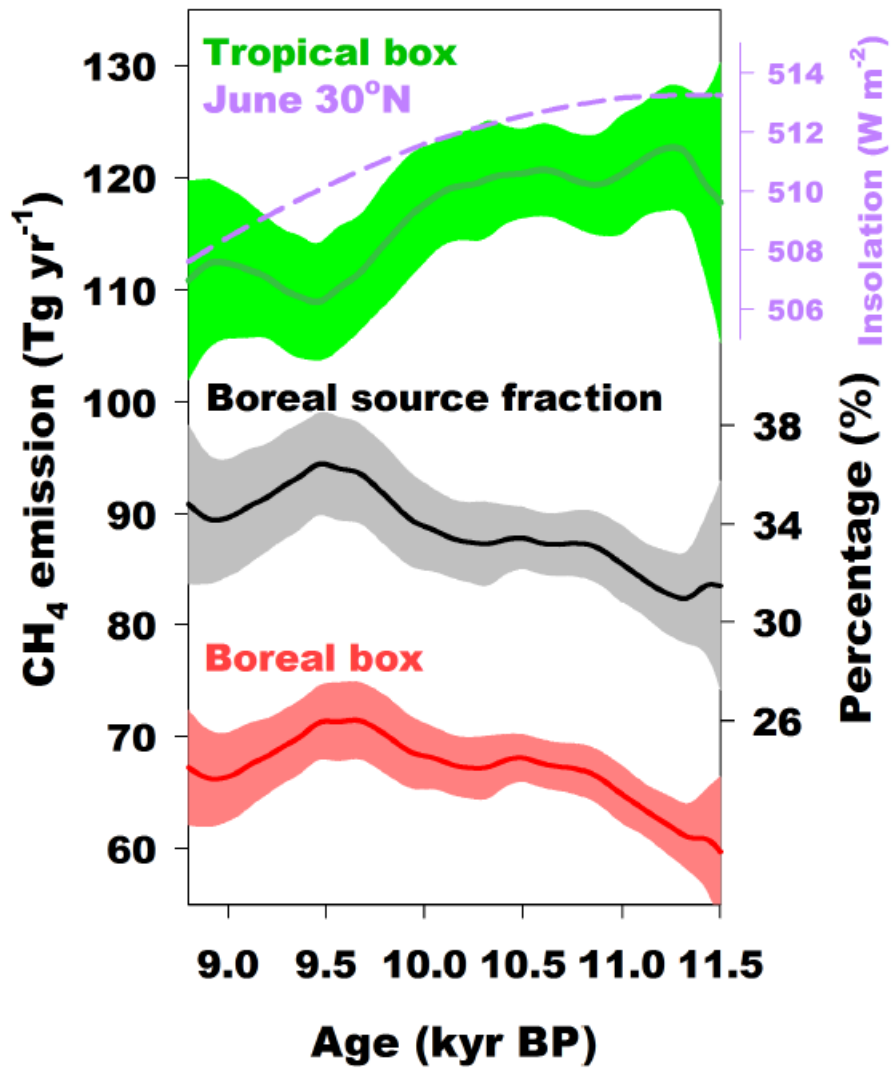
Figure 5. Comparison of Greenland oxygen isotope ratios from NGRIP (blue, Rasmussen et al., 2006), GRIP (grey, Rasmussen et al., 2006) and GISP2 (red, Stuiver and Grootes, 2000). All time series were high-pass filtered with 1/1800-year window. Note that the cooling amplitude at 10.3 ka is smaller than 8.2 and 9.3 ka events in NGRIP records, but this is not clear in GRIP and GISP2 ice cores.



1
 2 Figure 6. CH₄ inter-polar difference (IPD) and high latitude CH₄ sources. Top: High-resolution CH₄ discrete
 3 measurements from NEEM discrete (black, Chappellaz et al., 2013), NEEM continuous (orange, Chappellaz et al.,
 4 2013), WAIS Divide discrete (light blue, WAIS Divide project members, 2015), WAIS Divide continuous (green, Rhodes
 5 et al., 2015), and Siple Dome (red, this study) ice core records. Bottom: 1000-year low-pass filtered IPD
 6 reconstructions by using various pairs of Greenland- and Antarctic records, in which the IPD-1 and IPD-2 are shown
 7 in red and green, respectively. The shaded area indicate 95% significance interval.



1
 2 Figure 7. CH₄ inter-polar difference (IPD) and high latitude CH₄ sources. Top: High-resolution CH₄ discrete
 3 measurements from NEEM discrete (black, Chappellaz et al., 2013), WAIS Divide continuous (green, Rhodes et al.,
 4 2015), and Siple Dome (red, this study) ice core records. Middle: 1000-year low-pass filtered combined IPD with 95%
 5 significance interval (shaded). Bottom: Previous estimates are marked in green and orange (Brook et al., 2000;
 6 Chappellaz et al., 2013). Proxy-based temperature reconstruction for 30°N-90°N (purple, Marcott et al., 2013). CH₄
 7 flux estimate from Siberian- and Alaskan thermokarst lakes (red, Walter-Anthony et al., 2014).
 8



1
 2 Figure 8. 3-box source distribution model results of tropical (green) and boreal (red) boxes. Black line shows the boreal
 3 to total source fraction (see text). Purple dashed line plotted with tropical emission is summer insolation in 30°N (Berger
 4 and Loutre, 1991).
 5

1 **Table 1. Summary of results of replicate analysis from 8 depth intervals. Depth difference between the first- and second**
 2 **replicate samples is 10 cm.**

3

	1 st measurements					2 nd measurements				
Depth	Dup.1	Dup.2	Mean	1sigma	Date	Dup.1	Dup.2	Mean	1sigma	Date
(m)	(ppb)	(ppb)	(ppb)	(ppb)	(dd/mm/yy)	(ppb)	(ppb)	(ppb)	(ppb)	(dd/mm/yy)
523.150	634.8	634.7	634.7	0.1	27-1-14	637.5	634.3	635.9	1.6	24-2-14
530.950	669.0	665.8	667.4	1.6	03-2-14	669.4	670.7	670.0	0.7	24-2-14
558.295	682.5	678.2	680.3	2.2	14-3-14	687.5	678.3	682.9	4.6	02-4-14
559.850	689.8	680.3	685.0	4.7	03-2-14	683.8	690.0	686.9	3.1	26-3-14
561.150	687.8	689.2	688.5	0.7	14-3-14	684.0	690.4	687.2	3.2	02-4-14
562.407	687.2	685.5	686.4	0.8	26-3-14	689.4	686.4	687.9	1.5	02-4-14
575.913	679.2	679.2	679.2	0.0	07-2-14	686.7	678.9	682.8	3.9	28-3-14

4

5

1 **Table 2. Results of the 3-box source distribution model from the combined IPD showing emissions of tropical (green, T)**
 2 **and boreal (red, N) boxes and boreal source fraction ($N/(T+N+S)$) at specific time slices. Also shown are previous**
 3 **estimates for comparison. Errors denote 95% confidence interval. The uncertainty for 9.5 – 11.5 ka period is the average**
 4 **of 95% confidence interval of the low-pass filtered reconstruction of each box emission.**

5

Ref.	N box	T box	Boreal source fraction $N/(N+T+S)$
(ka)	(Tg yr ⁻¹)		(%)
Brook et al., 2000 (9.5-11.5 ka)	64 ± 5	123 ± 8	32 ± 3
Chappellaz et al., 1997 (9.5-11.5 ka)	66 ± 8	120 ± 9	33 ± 3
This study (9.5 – 11.5 ka)	67 ± 3	118 ± 5	33 ± 2
This study (11.5 ka)	60 ± 7	118 ± 12	31 ± 4
This study (9.5 ka)	71 ± 3	109 ± 5	36 ± 2
This study (9.0 ka)	66 ± 4	112 ± 7	34 ± 2

6

7